THE TEMPORAL AND SPATIAL DISTRIBUTION OF DISSOLVED AND PARTICULATE IRON OVER THE GULF OF ALASKA SHELF

By

Megan Victoria Roberts, B.S., M.S.

A Thesis Submitted in Partial Fulfillment of the Requirements

for the Degree of

Master of Science

in

Environmental Chemistry

University of Alaska

August 2018

APPROVED:

Ana M. Aguilar-Islas, Committee Chair
Thomas P. Trainor, Committee Co-Chair
William Simpson, Committee Member
Thomas K. Green, *Department of Chemistry and Biochemistry Chair*
Leah Berman, *Interim Dean of the College of Natural Sciences and Mathematics*
Michael Castellini, *Dean of the Graduate School*

Abstract

The Gulf of Alaska (GOA) is a region with contrasting ecosystems where the availability of the essential micronutrient iron (Fe) contributes to the observed productivity. However, knowledge on the temporal and spatial variability of iron species over the GOA shelf is limited. The offshore GOA displays lower annual production and residual nitrate in surface waters throughout the year due to low Fe supply, while high spring production is observed over the shelf due to ample nitrate and Fe supply, but these waters become nitrate limited by mid-summer. Processes promoting the exchange of the Fe rich shelf waters with the nitrate rich offshore GOA waters create favorable conditions for phytoplankton to bloom. Mechanisms for Fe introduction and transport are seasonal freshwater input, alongshore advection from the Alaska Coastal Current eddies, deep wintertime mixing, downwelling, downwelling relaxation, and/or upwelling conditions. Additional Fe sources from subsurface waters and sediment re-suspension can impact Fe distributions. Highly seasonal glacial and river input bring in an abundance of both particulate and dissolved Fe species, which differ in their biological availability. For example, dissolved Fe (DFe) is much more readily available than particulate Fe (PFe). The PFe pool can be separated into a labile fraction, which is potentially transferable to the dissolved phase on time scales relevant to phytoplankton blooms, and a refractory fraction, which is considered biologically unavailable.

Seawater samples to determine Fe speciation were collected in spring and early fall of 2013 during three GOA scientific cruises. Trace metal clean procedures were followed during sample collection, processing and analysis. Seawater samples were collected by two methods: 1) Vertical samples were obtained using custom-made samplers (UAF vanes) and filtered offline for PFe analysis; 2) surface samples were obtained by using a towed pump system ("the Fe fish") and filtered in-line for DFe analysis. The PFe fractions of suspended particles were further processed using chemical separation: a) 25 % acetic acid leach with a reducing agent to determine leachable particulate Fe; b) complete digestion of the filter using strong acids to determine refractory particulate Fe. Quantitative determination was by inductively coupled plasma mass spectrometry. Results indicate the broader Western GOA shelf displayed higher average concentrations of total particulate Fe (~121 nM on average) compared to the narrower Southeastern GOA shelf (~18 nM on average). Areas of high glacial input, such as in the vicinity of the Copper River discharge (western side of Kayak Island) and within Prince William Sound near Columbia Glacier, exhibited highly elevated concentrations of total particulate Fe (~430 nM to ~1100 nM). When comparing geographic location, the suspended leachable particulate Fe was higher (~ 22%) over the Southeastern shelf, while the Northern and Western shelf had lower percentage of leachable Fe (11 – 12 %). Over the Southeastern shelf, DFe concentrations were higher in late spring ranging (0.22 – 3.13 nM), while in early fall concentrations were lower (0.07 – 0. 84 nM). Surface water results indicate that there is a significant input of PFe and DFe that occurs in the early fall that extends over much of the Northern

shelf and at the inner Western shelf. Variability in downwelling, downwelling relaxation, and upwelling conditions were observed to impact Fe distributions over the Southeastern shelf. These results highlight the impact that the intense environmental variability characteristic of the GOA has on the distribution of Fe species seasonally and geographically.

Dedication Page

I dedicate this thesis: firstly, to my husband and children, for bearing with me through this challenging time, secondly, to my parents, who have loved and supported me through it all, and thirdly, to all the mothers pursuing higher education while having to maintain family and household responsibilities and maneuver the complex dynamics of life with children.

Table of Contents

List of Figures

Page

List of Tables

List of Appendices

Acknowledgements

I thank my advisor, Ana Aguilar-Islas, for sticking with me through the ups and downs of graduate school and for providing several semesters of research assistantships through the North Pacific Research Board's Gulf of Alaska Integrated Ecosystem Research Project (G84/F4185-00). She provided valuable guidance, critiques, and comments on my thesis that has strengthened my scientific writing. Additionally, she taught me how to have a critical eye towards research, which has strengthened my confidence in my professional scientific abilities. I thank my committee members, Tom Trainor (Co-Chair) and Bill Simpson, for their continued support, kind words, and guidance through stressful times. I would like to thank the Department of Chemistry and Biochemistry for supporting me through several semesters through teaching assistantships, which allowed me to develop and strengthen my science communication and teaching skills. I thank the Department of Biology and Wildlife for supporting me through one semester with a teaching assistantship. During my last semester, I had the opportunity to work as a research assistant for Kristin O'Brien. I would like to thank her for teaching me new molecular methods and being such an awesome person to work for—truly a good friend and boss. Also during my last semester, I was the recipient of an Instructional Design Fellowship with the eLearning Department that allowed me to use science and design to create educational content. It was a great experience! Thank you to the Instructional Design Team and specifically Kendell Newman Sadiik for being such an open, kind soul that provided valuable discussion that allowed new ideas to come to light.

Chapter 1: Introduction

1.1 Iron's role in primary production: In the global oceans and the Gulf of Alaska

The Gulf of Alaska (GOA) is a biologically rich region with contrasting ecosystems where the availability of the micronutrient iron (Fe) contributes to the observed productivity (Martin et al., 1989; Boyd et al., 2004). The GOA basin is a high nutrient but low chlorophyll (HNLC) system where residual nitrate is found through the year, but Fe concentrations are sufficiently low to limit primary production. In contrast, over the GOA inner shelf nitrate is depleted by summer, but waters remain rich in Fe (e.g. Lippiatt et al., 2010). Furthermore, the waters between these two contrasting ecosystems, the transition zone over the outer shelf and slope, is important for high primary production and CO_2 export (Palevsky et al., 2013), which impact fisheries and the global carbon cycle respectively. The essential micronutrient Fe restricts the growth of marine primary producers (phytoplankton) in approximately thirty percent of the surface waters in the global ocean, with the central GOA being one of those regions (Moore et al., 2002). Even though Fe is the fourth most abundant element of the Earth's crust (Taylor and McLennan, 1985), it is insoluble in near neutral pH, oxygenated seawater. This insolubility is due to the rapid precipitation of Fe to form iron oxides or hydroxides (Millero et al., 1995), creating an environment with open ocean surface Fe concentrations in the pico- to nanomolar (nM) range (Johnson et al., 1997).

Dozens of meso-scale Fe enrichment studies have demonstrated how this nutrient limits phytoplankton growth in the Fe depleted surface waters of the Southern Ocean, Equatorial Pacific, and Sub-Arctic Pacific, which encompasses the GOA (Martin and Fitzwater, 1988; Martin et al., 1994; Coale et al, 1996; Boyd et al., 2000; Boyd et al., 2007; de Baar et al., 2005). The addition of Fe to these low Fe systems fueled phytoplankton blooms in their natural environment. Because of its control on carbon fixing organisms this bioactive metal has been hypothesized to play a significant role in controlling atmospheric carbon dioxide concentrations on glacial to interglacial timescales (a.k.a. "The Iron Hypothesis", Martin 1990). The availability of Fe not only modulates phytoplankton growth but alters the algal community structure. Areas with high concentrations of Fe are dominated by larger phytoplankton species, such as diatoms, while in areas of low Fe, small phytoplankton species become more prevalent (Morel et al., 1991; Landry et al., 1997). This is important because diatoms are essential to the global carbon cycle as they are responsible for approximately 40% of primary production globally and sequestration/export of carbon due to the sinking of dead cells (Nelson et al., 1995; Armbrust et al., 2004; Field et al., 2011). Moreover, diatoms are key players in the biological pump being responsible for a percentage of the atmospheric CO_2 drawdown during glacial periods (Brzezinski et al., 2002). The availability of Fe has the potential to influence how marine primary producers adapt to the changing climate over long timescales and can influence primary production in shelf systems.

1.2 Biogeochemical cycling of iron in the marine environment

The distribution and speciation of Fe in coastal waters are dependent upon the dynamics of the system that can include seasonal freshwater input, spatially varying shelf morphology, and circulation patterns. Freshwater discharge delivers an abundant mixture of terrestrial particulates and dissolved material to coastal oceans. The fate of this material in the coastal environment depends on the amount and quality of the input (e.g., Hood and Scott, 2008; Schroth et al., 2011; Aciego, et al., 2015). The coastal GOA has a reliable input of Fe from the many rivers, streams, and tributaries that are influenced by precipitation, boreal forest, and glaciers (Hill et al., 2015). Streams influenced by glacial melt waters contain high loads of suspended glacial sediments rich in Fe, while streams more heavily influenced by their flow through boreal forests contain less sediment but more dissolved organic matter (Hood and Scott, 2008; Schroth et al., 2011). This mix of sedimentary particles and dissolved organic matter is how Fe and nutrients are actively transported from land into the coastal ocean. The fluvial input provides terrestrially derived macronutrients (carbon, nitrogen, silicon and phosphorous), as well as the micronutrient Fe to near shore waters (Hood and Scott, 2008; Schroth et al., 2011). The change in the salinity gradient from the river end member to saline waters plays a significant role on the stability of the particulate and dissolved material as the ionic strength is increased. For example, the size distribution of Fe is modified through the salinity gradient by physical settling of larger suspended particles and by removal of riverine dissolved Fe from flocculation along with humics (Sholkovitz et al., 1976). Due to Fe (III) being the thermodynamically favored species in seawater, hydrolysis occurs rapidly to form refractory mineral phases (solid iron oxides or hydroxides) that enhance the precipitation of Fe from the water column (Millero, 1998). This causes Fe to exhibit a non-conservative behavior across the estuary (Boyle et al., 1977). In GOA glacial estuaries, approximately ~ 85% of dissolved Fe is removed before reaching coastal waters over the shelf (Schroth et al., 2014). The continuous removal of dissolved Fe in seawater due to its tendency to form aggregates and/or adsorb to particles, results in seawater dissolved Fe concentrations that can become limiting to primary producers. However, a variety of other processes such as shelf sediment re-suspension and atmospheric deposition can enhance Fe concentrations in offshore waters. Over the GOA basin, the main source of Fe is seasonal atmospheric deposition via dust storms originating from glacially derived sediments (Crusius et al., 2011) and the Gobi desert (Zdanowicz et al., 2006; Yasunari et al., 2007), as well as transport of Fe rich shelf waters via meso-scale circulation patterns called eddies (Johnson et al., 2005; Lippiatt et al., 2011; Brown et al., 2012). Deep wintertime mixing can supply Fe from the re-suspension of shelf sediments (Lam et al., 2006). Thus, continentally derived Fe-rich particles can be transported long distances, up to 900 km offshore, which have the potential to trigger a phytoplankton bloom (Lam et al., 2006; Tsunogai et al., 1999). Additionally, shelf

waters are episodically resupplied through the seasons by Fe rich freshwater and glacial discharge which is advected alongshore with the Alaska Costal Current (ACC; more information regarding the ACC is in section 1.3) (Wu et al., 2009).

The two main Fe size classes presented in this thesis are dissolved and particulate Fe (Figure 1.1). Dissolved Fe (DFe) is considered to be readily accessible by phytoplankton uptake (Wells et al., 1995). The DFe size class includes all chemical forms of Fe < 0. 2 μm, which includes colloidal and "truly soluble" (< 0.02 μm) species that encompasses Fe bound by organic and inorganic ligands. Moreover, greater than 99 % of DFe is organically chelated (Buck et al., 2007). Association with dissolved organic ligands, such as siderophores produced by photosynthetic bacteria or dissolved organic matter, stabilizes dissolved Fe, and increases its residence time in surface waters (Barbeau, 2006). The particulate Fe fraction can be further characterized by differing chemical reactivity. The refractory fraction is biologically unavailable on timescales that are relevant for phytoplankton blooms and this includes suspended particulates that contain Fe in the mineral lattice of particles, such as glacial flour and other

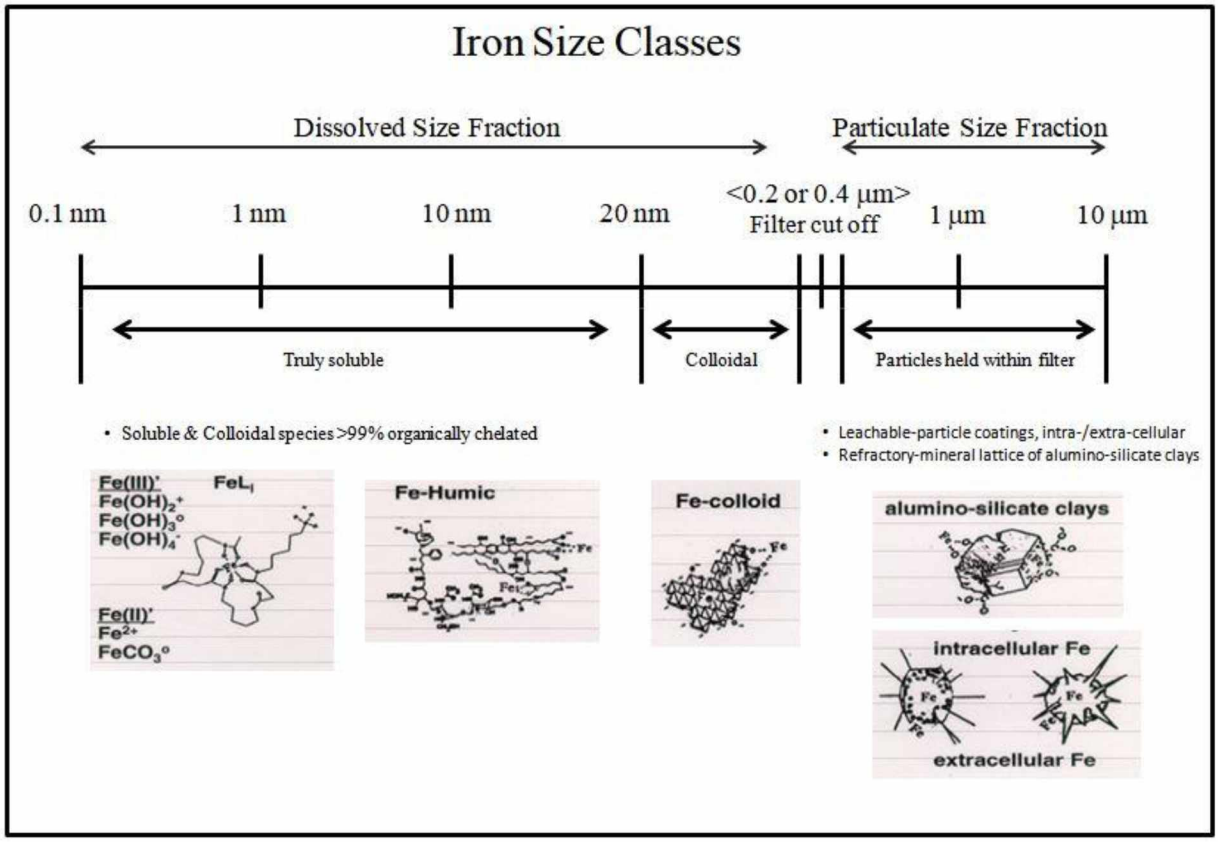

Figure 1.1: Visual depiction of the different iron size classes adapted from Bruland and Rue, 2001.

lithogenic sediment. The leachable particulate fraction includes the Fe that is found intra-cellularly in biogenic particles or that is adsorbed to the outer coatings of both lithogenic and biogenic particles. The leachable particulate Fe fraction is considered reactive, or labile, and has the ability to be transferred into the dissolved pool on short time scales (weeks to months) (Berger et al., 2008). In coastal waters, the mechanism for the transfer from particulate to dissolved can occur through ligand assisted dissolution (Buck et al., 2007), diagenic reductive dissolution (Elrod et al., 2004), non-reductive dissolution (Radic et al., 2011), and photolysis (Roy et al., 2008). The ability of suspended particles to house leachable Fe will depend upon the types of chemical or physical weathering that the particle has been exposed to, i.e. re-suspended shelf sediments that have undergone reductive process and subsequent re-oxidation (Hurst et al., 2010) versus glacial or river derived sediments where surface areas can contain variable loadings of Fe oxides (Poulton and Raiswell, 2005). To better understand the biogeochemical cycling of the micronutrient Fe in the GOA region, studies have focused on identifying spatial and temporal distributions of the differences in Fe size partitioning in glacial versus boreal streams (Schroth et al., 2011), in surface waters across the Western shelf in spring and summer (Wu et al., 2009), in coastal waters versus river plumes during summer (Lippiatt et al., 2010), as well as seasonal differences in coastal surface waters (Aguilar-Islas et al., 2016).

1.3 Gulf of Alaska physical setting

The GOA is framed by mountains that are characterized by boreal forests and glaciers and serve as the interface between land and ocean. Within this interface, there is a complex network of fjords and sounds that receive a highly seasonal discharge of sediment laden freshwater from a vast system of small rivers and streams draining snow and glacial melt waters (Christensen et al., 2000; Mote et al., 2003; Hill et al., 2015). The streams and rivers that are broadened by this runoff will reach their peak discharge between late summer and early fall, thus transporting the particulate laden freshwater to the narrow, swift and coastally trapped ACC, which is characterized by a low salinity core that creates a cross shelf density gradient (Royer, 1987; Stabeno et al., 2004). The ACC is a buoyant, density driven flow that entrains Fe rich waters and transports them counter clockwise along the inner GOA shelf. The ACC is bordered by the dominant offshore flow of the Alaska Current and Alaskan Stream (Stabeno et al., 2004; Wu et al., 2009) (Figure 1.2). Through the low fluvial input seasons of winter and spring, the salinity core of the ACC remains relatively fresher than the surrounding waters (Stabeno et al., 2004). However, the ACC is not a continuous feature along the length of the GOA shelf. In the Southeast, the ACC is less defined but has general northwestward flow. Here, the ACC starts at the southern tip of Baranof Island and continues to Cross Sound (defined herein as the Southeastern shelf) where it is broken up by a deep canyon (Yakobi Valley) and resumes again northwest of Yakutat Bay (part of the Northern shelf) (Stabeno et al., 2016a).

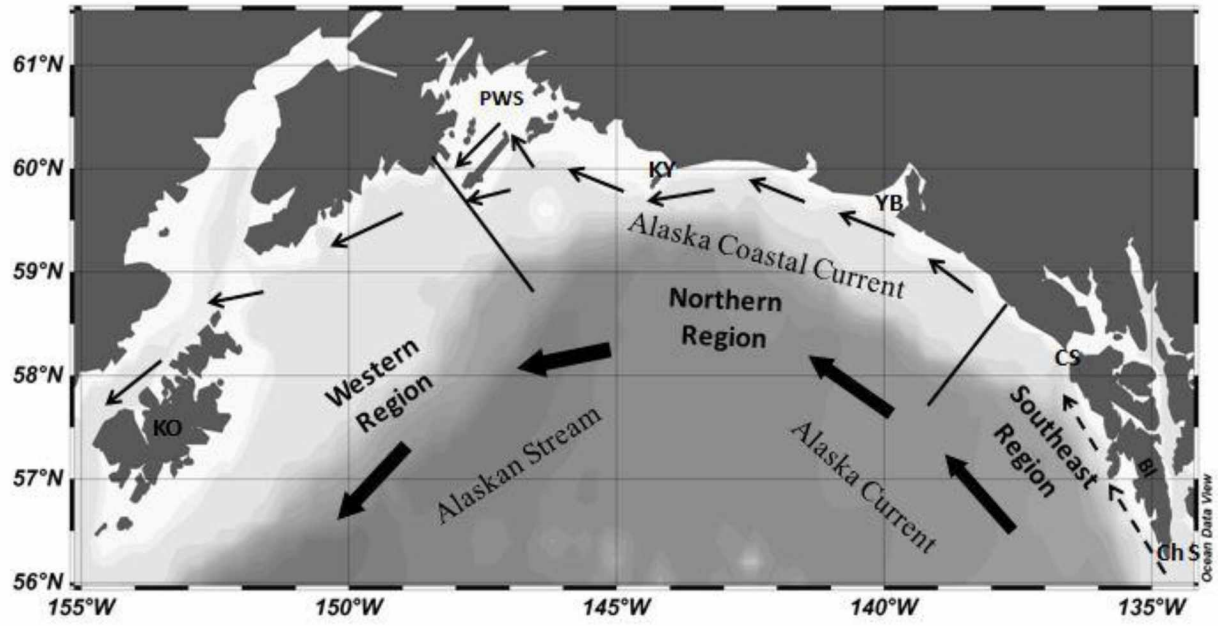

Figure 1.2: Map of the Gulf of Alaska shelf and offshore circulation patterns. The shelf circulation is dominated by the Alaska Coastal Current, which is not well defined over the Southeastern shelf (dashed arrows) but resumes again near Yakutat Bay (solid arrows). The offshore Gulf of Alaska is influenced by the Alaska Current and Alaskan Stream. Chatham Strait (Ch S), Baranoff Island (BI), Cross Sound (CS), Yakutat Bay (YB), Kayak Island (KY), Prince William Sound (PWS), and Kodiak Island (KO) are indicated.

Further along the Western shelf, the ACC is mostly continuous at the inner shelf on the northern side of Kodiak Island. On the southern side of Kodiak Island, there is complex mixing and influences from the Alaskan Stream. In addition to the ACC, the GOA shelf supports oceanographic processes that yields cross shelf exchange of waters between the basin and shelf that are important in exchange of nutrients. Cross shelf exchange has been identified to occur by three primary mechanisms: downwelling relaxation, eddies, and bathymetric steered tidal mixing (Stabeno et al., 2004; Ladd et al., 2005). The GOA is a predominantly downwelling system throughout the year but episodic upwelling occurs in the summer that introduces nutrient rich but Fe poor basin waters onto the shelf (Martin et al., 1989; Ladd et al., 2005). The continental shelf in the GOA is interjected with multiple underwater canyons that create an environment where the water column can be complexly mixed and redirected, promoting an exchange of basin waters with shelf waters (Ladd et al., 2005). In addition, shelf waters can be transported by eddies propagating along the northern and southeastern shelf. These entrain Fe rich shelf waters transporting it in a westerly fashion into the nitrate rich central GOA basin (Ladd et al., 2009). The GOA shelf also

experiences deep wintertime mixing that allows for the opportunity to resuspend shelf sediments that can further enhance Fe concentrations the water column (Lam et al., 2006).

This study divides the GOA shelf into three regions: the Southeastern shelf, Northern shelf, and Western shelf (Figure 1.2). The Southeastern shelf extends from the southern end of Baranof Island near Chatham Strait to northward of Cross Sound. This part of the shelf is very narrow (< 20 km) and receives ~ 43 % of the mean annual freshwater runoff that enters the GOA, which is a result of the intense low pressure systems in this area that produce significant amounts of precipitation (Weingartner et al., 2005; Neal et al., 2010). The Northern shelf begins midway between Cross Sound and Yakutat Bay, where the shelf begins to widen and extends to the left of Kayak Island ending before Prince William Sound (PWS). Freshwater discharge is from the Copper River and Alsek River (mean annual freshwater runoff: ~31 % of total), which influence near shore waters with large loads of river and glacial sediments (Naidu and Mowatt, 1983; Christensen et al., 2000; Neal et al., 2010). The Western shelf is significantly wider than the other regions (> 200 km) but receives less freshwater discharge that contributes only ~ 17% to the total GOA runoff (Neal et al., 2010).

1.4 Study objectives

The aim of this thesis is to characterize dissolved and particulate Fe over the GOA shelf and to better constrain the understanding of how freshwater input, oceanographic processes, and shelf geomorphology impact the distribution and speciation of Fe in surface waters and at depth. The study was funded by the North Pacific Research Board and is part of a larger project (Gulf of Alaska Integrated Ecosystem Research Program, GOIERP) that is aimed at understanding recruitment in five commercially important fisheries. The Gulf of Alaska sustains wholesale fisheries commodities worth $4.6 billion (Northern Economics, Inc., 2011). The Fe work presented here adds to the knowledge of the dynamics of the micronutrient Fe for reactive and particulate Fe species both at the surface and at depth over a large portion of the GOA shelf. Discussion topics will include variability in the observed Fe distribution in time (seasonal and interannual) and space (cross shelf and along shelf), and the factors that contribute to the observed variability. Overall, this work contributes to the understanding of the GOA shelf ecosystem.

Chapter 2: The temporal and spatial distribution of dissolved and particulate iron over the Gulf of Alaska shelf.[1]

Abstract

The micronutrient iron (Fe) plays a significant role in modulating the primary production in the offshore waters of the central Gulf of Alaska (GOA), while at the inner shelf the availability of the macronutrient nitrate is a major influence on primary production. Between these two regimes the relative availability of these two nutrients affects phytoplankton community composition and abundance. Biological availability of Fe is related to the size and chemical reactivity of Fe species present in seawater. Glacial and riverine input rich in dissolved and particulate Fe species is transported along the GOA inner shelf by the swift moving Alaska Coastal Current (ACC). Freshwater input of Fe is highly seasonal and tends to remain trapped within the ACC. Thus, the GOA shelf exhibits Fe concentration gradients that differ by orders of magnitude. Previous studies have identified freshwater input and meso-scale eddy activity as important processes affecting the variability in Fe chemical species over the GOA shelf. The objectives of this study were to identify the temporal (seasonal and inter-annual) and spatial (along-and cross-shelf) distribution of Fe over a large region the GOA shelf (from Chatham Strait to Kodiak Island), and to investigate differences in regional and seasonal processes responsible for the observed Fe distributions. Results support previous observations, and indicate that shelf geomorphology (i.e., bathymetric features and shelf width) in combination with physical process (e.g., vertical mixing by storms and timing of fresh water input) lead to differences in the concentration, size partitioning and chemical reactivity of Fe over the GOA shelf. Results indicate freshwater input over the Southeastern shelf increases reactive Fe in surface waters in the spring that contrast to the early fall when significant decreases in concentrations were observed. Concentration gradients were observed across the Northern shelf (~ 800 nM to < 50 nM) where the Copper River discharges and across the GAK Line over the Western shelf (~ 250 nM to < 15 nM). Variability in downwelling (and relaxation) and/or upwelling conditions impacted Fe distributions along the Southeastern shelf and slope. In the early fall, when freshwater input is at its peak, dissolved Fe concentrations increase drastically over much of the Northern and Western shelves.

[1]Roberts, M.V., A.M. Aguilar-Islas. The temporal and spatial distribution of dissolved and particulate iron over the Gulf of Alaska shelf. Prepared for submission to Marine Chemistry.

2.1 Introduction

The Gulf of Alaska (GOA) presents two contrasting ecosystems, i.e. the central GOA is a high nutrient but low chlorophyll (HNLC) system where primary production is limited by the availability of

iron (Fe) (Martin et al., 1989; Boyd et al., 2004) while continental shelf waters are rich in Fe and the relative availability of Fe to nitrate contributes to the observed productivity here (Strom et al., 2007; Wu et al., 2009; Lippiatt et al., 2010; Aguilar-Islas et al., 2016). Deep wintertime mixing allows macro- and micronutrient rich subsurface water to be mixed throughout the water column (Childers et al., 2005; Aguilar-Islas et al., 2016). Winter mixing can also potentially supply Fe from re-suspended shelf sediments priming waters for the spring phytoplankton bloom (Lam et al., 2006). Across the shelf and slope after the spring bloom, waters become nitrate limited by mid-summer, but due to downwelling relaxation there can be an onshore flux of nutrient dense bottom water to the inner and mid shelf (Childers et al., 2005). During summer and fall, input of Fe to shelf waters is largely from freshwater, which has its peak discharge in late summer and early fall (e.g. Hill et al., 2015).

The GOA is surrounded by mountains that drain a mixture of boreal forests and glaciers that receive high amounts of precipitation. The subsequent snow and glacial melt produces a seasonally variant runoff (Mote et al., 2003; Hill et al., 2015). The particulate laden freshwater to discharges along the coast where it joins the swift, alongshore Alaska Coastal Current (ACC) (Royer, 1987; Stabeno et al., 2004). The density driven ACC starts over the narrow (< 20 km) Southeastern shelf near the tip of Baranoff Island and is briefly interrupted near Cross Sound by deep underwater canyons. It resumes again at the broadening Northern shelf near Yakutat Bay and is mostly continuous along the wider (> 200 km) Western shelf (Stabeno et al., 2004). The ACC transports Fe rich waters along the inner shelf but complex wind forcing, eddies and meanders of the shelf/slope current system create cross shelf gradient of Fe concentrations (Ladd et al., 2009; Wu et al., 2009; Brown et al., 2012). During the late winter and early spring prior to freshwater input, surface concentrations of dissolved Fe (DFe) appear to be insufficient for biological demand in relation to the available nitrate over much of the shelf (Aguilar-Islas et al., 2016). Through the summer and early fall, speciation is dominated by the particulate Fe (PFe) fraction due to the large particulate input from glacier influenced runoff (Lippiatt et al., 2010). During fall an additional Fe source is glacially derived dust that can be transported long distances over the GOA shelf and deposit in the central GOA (Crusius et al., 2011). Here, we present new data that highlight the seasonal and spatial variability in the partitioning of Fe over a broad region of the GOA shelf.

2.2 Materials and methods

2.2.1 Sampling region

Field samples were collected in 2013 during three scientific cruises, two in late spring (April 8 - 23 on board the NOAA Ship *Oscar Dyson* (DY); April 26 - May 6 on board the R/V *Tiglax* (1TX)), and

Table 2.1 Cruise name, dates and location, sample collection methods and Fe species analyzed.

Cruise Name	Dates	Location	Samples Collection Method	Fe Species
DY	4/8/13 - 4/23/13	Southeastern & Northern	Vertical Profiles (UAF Vane) & Surface (Fe Fish)	DFe, LPFe, RPFe, TPFe
1TX	4/26/13 - 5/6/13	Northern & Western	UAF Vane & Fe Fish	DFe, LPFe, RPFe, TPFe
2TX	9/16/16 - 9/26/13	Southeastern, Northern, & Western	Fe Fish	DFe, LPFe, RPFe, TPFe

one in early fall (September 16 - 26 on board the R/V *Tiglax* (2TX)) (Table 2.1). Surface seawater was sampled over the Southeastern, Northern, and Western GOA shelf during the three cruises (Figure 2.1). Surface seawater was collected in the late spring along 11 transects spanning over the Southeastern (off the southern end of Baranoff Island and northward to Cross Sound), Northern (from northwest of Cross Sound to southeast of Kayak Island), and Western shelves (from the bottom tip of Montague Island to off the coast of Kodiak Island) (Figure 2.1b). Fall surface seawater collection was obtained from 10 transects that covered similar areas to the ones sampled in spring, and an additional single sample was obtained from PWS north of Columbia Bay (Station CB) (Figure 2.1c). Vertical profiles were obtained in the late spring and included samples from stations over the Southeastern shelf and slope (Transects SEA, SEG, and SEK), the Northern Shelf near Yakutat Bay (Transects YBC and YBE), Kayak Island (Stations KIA and KIB) and within Prince William Sound (PWS) near the Columbia Glacier (Station CG), and the Western shelf along the Seward Line (GAK Line), and near Kodiak Island over the shelf and slope (Stations181-HL, 185-HX, 197-HL, and 197-HT) (Figure 2.1a). The distance from shore is denoted in the station name for the Southeastern and some of Northern shelf samples, i.e. SEA 5 is approximately 5 kilometers from shore and YBC 10 is approximately 10 kilometers from shore. Stations near Kayak Island and along the Western shelf follow naming conventions from NOAA's Fisheries-Oceanography Coordinated Investigations.

2.2.2 Sampling protocols

All sample collection and processing were conducted using trace metal clean procedures recommended by the International GEOTRACES Program. Specific information can be found at (http://www.geotraces.org/science/intercalibration/222-sampling-and-samplehandling-protocols-for-geotraces-cruises). Sample collection protocols were similar to those previously described in Aguilar-Islas et al. (2016). Briefly, surface seawater samples were obtained with the use of trace metal clean towed

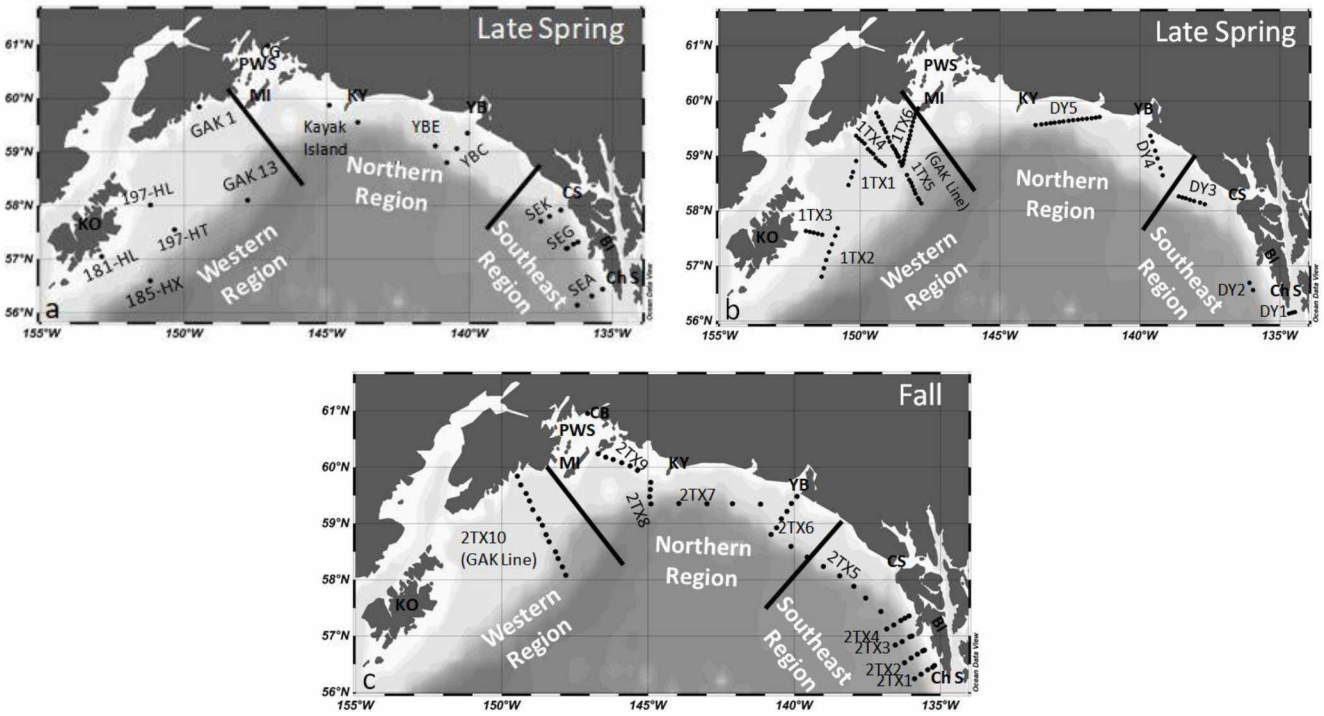

Figure 2.1: Stations and transect names sampled in the Gulf of Alaska for dissolved and particulate iron. Vertical profile station during late spring (a), surface transect during late spring (b), and early fall (c) are indicated by circles. The sampling regions are divided into the southeast, northern, and western shelf regions as indicated by the black solid lines. Chatham Strait (Ch S), Baranoff Island (BI), Cross Sound (CS), Yakutat Bay (YB), Kayak Island (KY), Montague Island (MI) Prince William Sound (PWS), Columbia Glacier (CG), Columbia Bay (CB), and Kodiak Island (KO) are also label on the maps.

pump system (Bruland et al., 2005; Aguilar-Islas and Bruland, 2006), referred herein as "the Fe fish". Surface samples from the towed system were filtered in-line through a 0.2 μm pore Supor Acropak 200 filter capsule (Pall Corporation) that was rinsed with at least 10 L of seawater prior to use. The filtered surface seawater was pumped aboard into a positive pressure clean space within a plastic enclosure constructed inside the ship's lab (NOAA *Oscar Dyson),* or inside a clean van (R/V *Tiglax*). Dissolved Fe (DFe) was obtained from these samples (see section 2.3 for sample processing). Surface water temperature and salinity were obtained from the ships' underway system.

Vertical profiles were obtained using University of Alaska Fairbanks (UAF) vanes (Wu, 2007; Wu et al., 2009) attached at least 10 m above the CTD Rosette on the hydrowire. The UAF vanes are a modified version of the Moored In-Situ Trace Element Serial Sampler (MITESS, Bell et al., 2002). The MITESS module is attached to a 2 L polyethylene bottle mounted on a plastic vane. The MITESS module is pre-programmed to open and close at a given depth while the vane directs the assembly to align with the current and position the bottle upstream of the hydrowire to allow for collection of uncontaminated

seawater. Total particulate Fe (TPFe), refractory particulate Fe (RPFe), leachable particulate Fe (LPFe), and DFe were obtained from these samples (see sections 2.3 for sample processing). Water column temperature, salinity, and beam transmission were obtained from sensors on the CTD Rosette. Chlorophyll biomass was sampled by the Strom Lab (Western Washington University) during the same time as the vertical profiles were obtained. A portion of the sample data was published by Strom et al. (2016) but some of the chlorophyll biomass data included here are unpublished.

2.2.3 Sample processing

Filtered Fe Fish samples were collected into pre-cleaned low density polyethylene (LDPE) bottles, acidified to pH < 2 (Optima grade HCl, Fisher Scientific; 2 ml concentrated HCl/L) upon return to the laboratory, and analyzed (see section 2.3.1) after one month of storage at room temperature. For suspended particles, unfiltered seawater samples (~ 1 – 1.5 L) were vacuum filtered onboard inside the clean space through pre-cleaned 47 mm diameter 0.4 um track etched polycarbonate filters (Nuclepore). The filtered water was used for DFe analysis and processed as the Fe fish samples. The filters with suspended particles were folded into eighths and placed into pre-cleaned, acid washed, 7 mL polypropylene (PP) vials. Blank filters were treated the same as samples, but using ultra pure (Milli-Q) water (18.2 MΩ cm) instead of seawater. The filters were frozen at – 20° C, transported frozen to the UAF trace metal laboratory, and thawed prior to processing. Particles were sequentially processed to first obtain the LPFe fraction, and the remaining RPFe fraction. The leachable fraction was separated with a modified version of the leach method recommended by Berger et al. (2008). Briefly, the filter samples were subjected to a 25% acetic acid (Optima grade, Fisher Scientific) heated solution containing the reducing agent, hydroxylamine hydrochloride (0.2 M). With this leach, intracellular Fe is released during the heating step and the reducing agent aids in the leaching of Fe associated with particle surfaces, like oxy-hydroxides (Berger et al., 2008). The protocol was as follows: The leach solution (1.5 mL) was added to the 7 mL PP vials containing the thawed filters. These were kept upright and positioned into a heated water bath at approximately ~ 90° C for 10 minutes. The filters were then left to cool to room temperature (~ 30°C) for two hours. At the end of the leaching period, the leachate was transferred to 2 mL centrifuge vials and centrifuged for 0.5 minute at 8 rpm. This is a modification from the Berger et al. (2008) method, and it was done to separate particles potentially transferred from the filters into the leachate. After centrifugation, the leachate was transferred to a Teflon beaker and the centrifuged particles were stored until further processing. The 7 mL PP vial walls were carefully rinsed 3 times with 300 µL of Milli-Q and transferred to the same Teflon beaker with leachate. The beakers were heated to dryness and 100 µL of HNO_3 (high purity distilled nitric acid) was added to re-suspend the residue. Milli-Q water (1.5 mL) was added and the solution was transferred to a clean 7 mL vial. Beakers were triple rinsed with 500 µL of 1

M HNO_3. The concentration of the final HNO_3 (1 M) is used as the matrix for quantitative analysis. Leached filter samples and remaining particles from the modified leach method were then digested sequentially with strong acids (HNO_3, HCl, HF) (Optima Grade; Fisher Scientific) and hydrogen peroxide (H_2O_2) (Optima Grade; Fisher Scientific) to obtain the refractory fraction. Filters were placed in Teflon vials (10 mL, Savillex), 1 mL of concentrated HNO_3 and 0.5 mL of concentrated HCl were added, and capped vials were heated overnight (approximately 12-14 hours; ~ 80°C). A second concentrated acid solution (1 mL HNO_3, 0.5 mL HCl, and 0.2 mL HF) with hydrogen peroxide (0.2 mL H_2O_2) was added. The vials were loosely capped and heated overnight (~ 80°C) and followed with heating to dryness. After drying, the final digested sample was diluted with concentrated HNO_3 (1 mL) and rinsed with Milli-Q (10 mL). The diluted sample was then transferred to 7 ml PP vial before quantitative analysis. Blank filters were treated the same as samples. Reagent blanks were processed during the digestions using the same protocol.

2.2.4 Quantitative analysis

Analyses were conducted at the University of Alaska Fairbanks. The concentrations of DFe and TDFe were quantified by isotope dilution using high resolution inductively coupled plasma-mass spectrometry detection (HR-ICP-MS; Thermo Fisher Element2) after a modified version of the Lagerström et al. (2013) on-line method. Briefly, acidified samples were spiked with a solution of ^{57}Fe in 0.16 M HNO_3 (Optima grade) and using an automated flow-injection system (seaFAST, ESI) the sample pH was buffered with ammonium acetate (Optima grade) for concentration onto the seaFAST chelating resin and subsequent elution with 1.6 M HNO_3 (Optima grade) directly into the Element 2 mass spectrometer. A total of 4 ml of sample were concentrated onto the resin, and quantification was based on the elution peaks of ^{57}Fe and ^{56}Fe, which were generated from the initial 150 µl of eluted solution. Procedural blanks for DFe are negligible using the UAF seaFAST system, which has been continuously cleaned over several years. The accuracy (< 3%) and precision of the method were evaluated by analyzing SAFe reference seawater. Accuracy was determined from the analysis of the reference sample SAFe D2 (0.923±0.008 nM; n=13) which was within the latest community consensus value (SAFe D2 = 0.933±0.023 nmol/kg) reported in May, 2013 (www.geotraces.org). Suspended LPFe and RPFe were determined by direct injection into the mass spectrometer as described by Aguilar-Islas et al., (2013). Quantification was achieved with the use of external standards. Single element standards were diluted into a 1 M HNO_3 matrix from a primary stock of 1000 ppm (Perkins & Elmer) to create an external standard curve (0-105 ppb) and gallium was used as an internal standard. Samples were further diluted in a 1 M HNO_3 matrix as required to quantify the leachable and refractory particulate Fe and aluminum (Al). Aluminum was used as a tracer of lithogenic material (see section 2.4.4). Values are

reported in nanomole of Fe (Al) per L of filtered seawater (nM) with the subtraction of the filter and reagent blanks.

2.3 Results

2.3.1 Late spring

2.3.1.1 Surface dissolved Fe distributions

Surface water salinity, temperature, and DFe are shown in Figure 2.2. Generally, salinity was fresher (~ 31.5) closer to shore, where the ACC is present, and increased offshore (~ 32 to 32.5) along the surveyed shelf regions. Within PWS, salinities were as low as ~ 29. Along the wider Western shelf salinities were higher (~ 32 to 33) than the narrow Southeast shelf, where the observed salinity was below 32. Temperatures were warmer over the Southeastern shelf (~ 6 to 7°C) and cooler over the Northern and Western shelf (~ 5 to 6°C). Waters sampled over the Southeastern and Northern shelf (Transects DY1–DY5) span the region from the bottom of Baranoff Island to northwest of Yakutat Bay. At Transect DY1 (April 14), relatively elevated concentrations of surface DFe from 2.02 to 2.64 nM were observed across the length of this transect. Lower surface DFe were observed further north along Transects DY2 (April

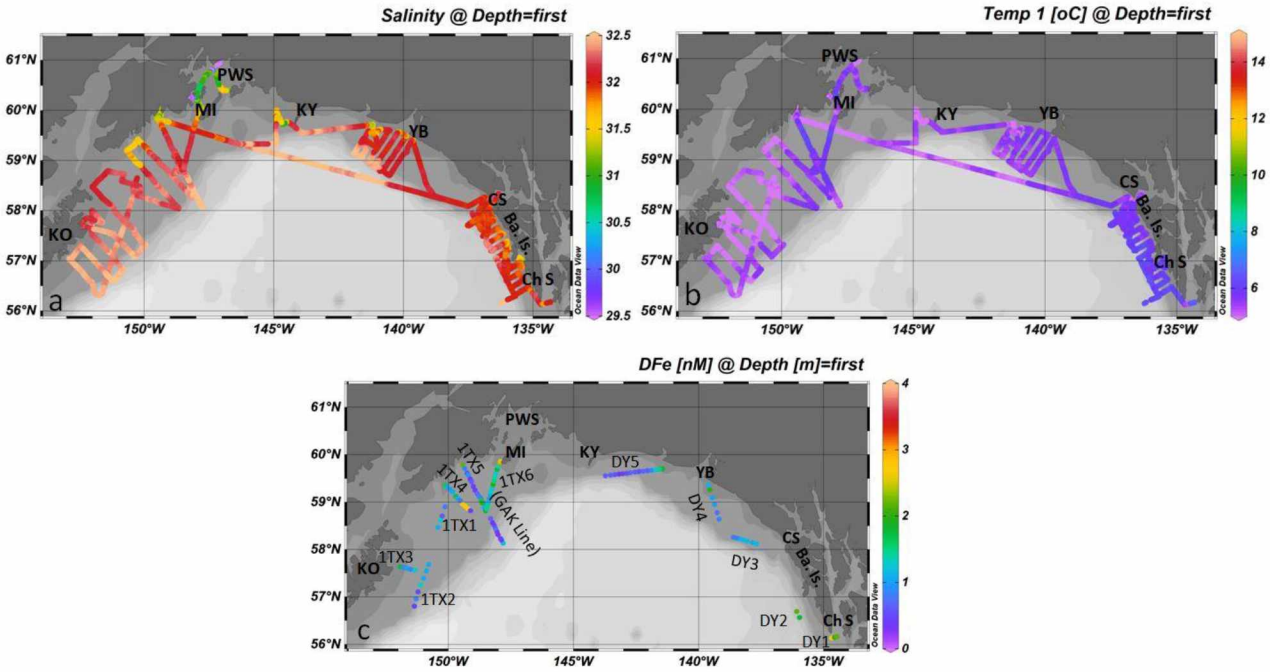

Figure 2.2: Maps of the surface transects during late spring 2013 along the Gulf of Alaska shelf. Temperature (a) and salinity (b) were obtained from the ship's underway system. Samples for the analysis of dissolved Fe (c) were obtained from the trace-metal-clean towed system.

16) and DY3 (April 18), where DFe concentrations decreased from an average of 1.82 nM along DY2 to 1.01 nM along DY3. Along Transect DY4 (April 19) the cross shelf gradient increased in surface DFe as this transect approached Yakutat Bay, from 0.79 near the outer shelf to 2.84 nM near the mouth of the bay. Transect DY5 (April 22) showed similar pattern of elevated concentrations over the inner shelf, from 1.79 to 1.50 nM, then decreasing across the outer shelf (ranging from 0.38 to 0.65 nM). Surface water along the Western shelf (Transects 1TX1, 1TX2, and 1TX3) had DFe concentrations that did not exceed 1.71 nM and this concentration was found at Transect 1TX3. Elevated DFe (~2.7 nM) was found near the end of Transect 1TX4 which coincided with fresher salinity (~ 31.5) closer to the shore. At Transect 1TX5 (GAK Line), DFe was as high as 2.17 nM but decreased rapidly to 0.34 nM. Over the mid-shelf, elevated DFe concentrations (~1 to 2 nM) were observed. At the end of Transect 1TX5 DFe decreased from ~ 0.77 to 0.29 nM. The Transect 1TX6 extended from the mid GAK Line northeast to meet the southwest end of Montague Island (MI). The average DFe along this transect was 1.52 nM with the highest concentration (2.86 nM) found near MI, and the lowest (0.96 nM) observed closer to the GAK Line.

2.3.1.2 Vertical profiles: Southeastern shelf

Depth profiles for DFe, LPFe, TPFe, salinity, temperature, beam transmission, and chlorophyll a (Chl a) for the Southeast shelf are shown in Figures 2.3 – 2.5. Over the Southeast shelf between April 8 – 17, 2013, samples were obtained from transects SEA, SEG, and SEK. Sampled stations were between 5 and 40 kilometers from shore as designated in their names (e.g. SEA 5 or SEK 30). Salinity and temperature cross-shelf gradients at 20 m reflect those observed in surface water (see Section 2.3.1.1). Fresher and cooler waters (~ 31.9 and 5.8°C) were observed at SEA 5, while at SEA 40 waters became more saline and warmer, (~ 32.6 and 6.3°C) . Water depth along Transect SEA increased rapidly from 120 m at SEA 5, to 1091 m at SEA 20 , and 2390 m at SEA 40. At SEA 5, salinity increased to 32.7 and temperature decreased to 5.5°C in bottom waters. Here beam transmission and Chl a covaried with depth; as Chl a decreased from a maximum of 0.64 μg/L at the 20 m to 0.11 μg/L at 70 m, beam transmission increased from ~ 95 % at 20 m to ~ 98 % at 70 m. At Station SEA 20 and SEA 40 covariability between Chl a and beam transmission was also observed (Figures 2.3 e, h). There were elevated amounts of particulate Fe at Stations SEA 5 and SEA 20, while a ten-fold decrease in this Fe fraction was observed at the offshore station, SEA 40 (Figure 2.3). At Station SEA 5, TPFe increased with depth to 46 nM at 100 m, which was approximately three times the amount observed at 15 m (~16 nM). Dissolved Fe was observed to be variable ranging from 1.94 nM to a subsurface maximum of 3.9 nM at 75 m. The LPFe fraction at Station SEA 5 was variable ranging from 22.5 – 42.6 % of the TPFe with the highest percentage at 50 m. At Station SEA 20, the TPFe and DFe remained relatively homogenous throughout

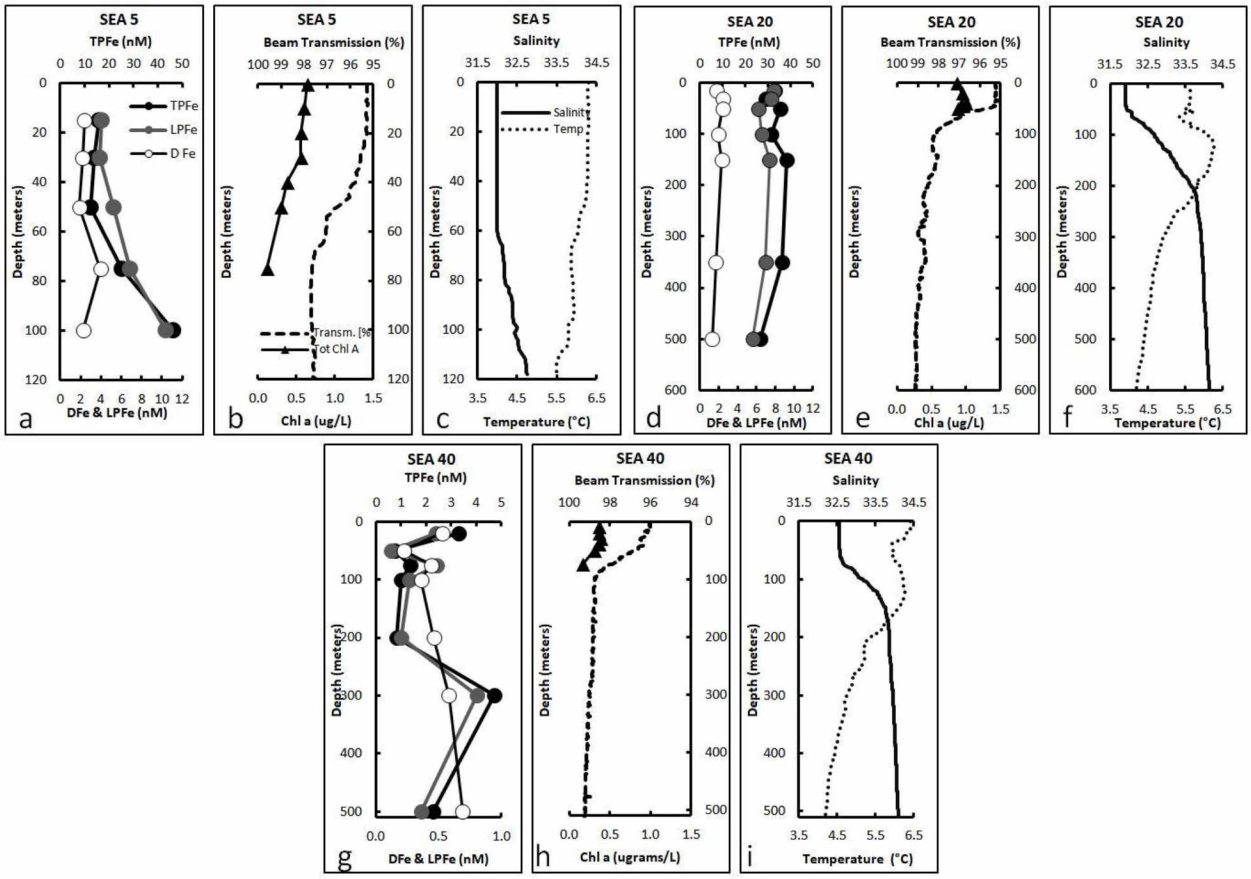

Figure 2.3: Vertical depth profile plots at Stations SEA 5, SEA 20, and SEA 40. DFe (white circles), LPFe (gray circles), TPFe (black circles) (a, d, g) were collected using UAF vanes deployed above the CTD rosette. Beam transmission (%) (b, e, h), salinity and temperature (c, f, i) were collected from sensors on the ship's CTD rosette. Chlorophyll a (b, e, h) was provided by the Strom Lab.

the water column with TPFe concentrations ranging between 26.5 and 38.3 nM, while DFe ranged from 1.3 nM to 2.4 nM. The concentration of LPFe also varied narrowly from 5.6 nM to 7.8 nM, but the percent of the LPFe fraction was variable, representing 17.5 % to 26 % of the TPFe, with highest percentage observed in the mixed layer at 30 m. The offshore station, SEA 40, was sampled at depths between 20 and 500 meters. The water column exhibited low concentrations in both TPFe and DFe with an average of 2.03 nM and 0.47 nM, respectively. The concentration of LPFe was an order of magnitude less at SEA 40 with values at or below 0.8 nM. The percent LPFe fraction remained similar to that at SEA 20 (on average ~ 21 % of the TPFe).

Temperature and salinity at the inner shelf along Transect SEG (Station SEG 5) varied little with depth, with salinity increasing from 32 to 32.8 and temperature ranging from ~ 6.0 to 6.5°C (Figure 2.4). Here, beam transmission at the surface was the lowest observed (77 %) during the cruise, but quickly

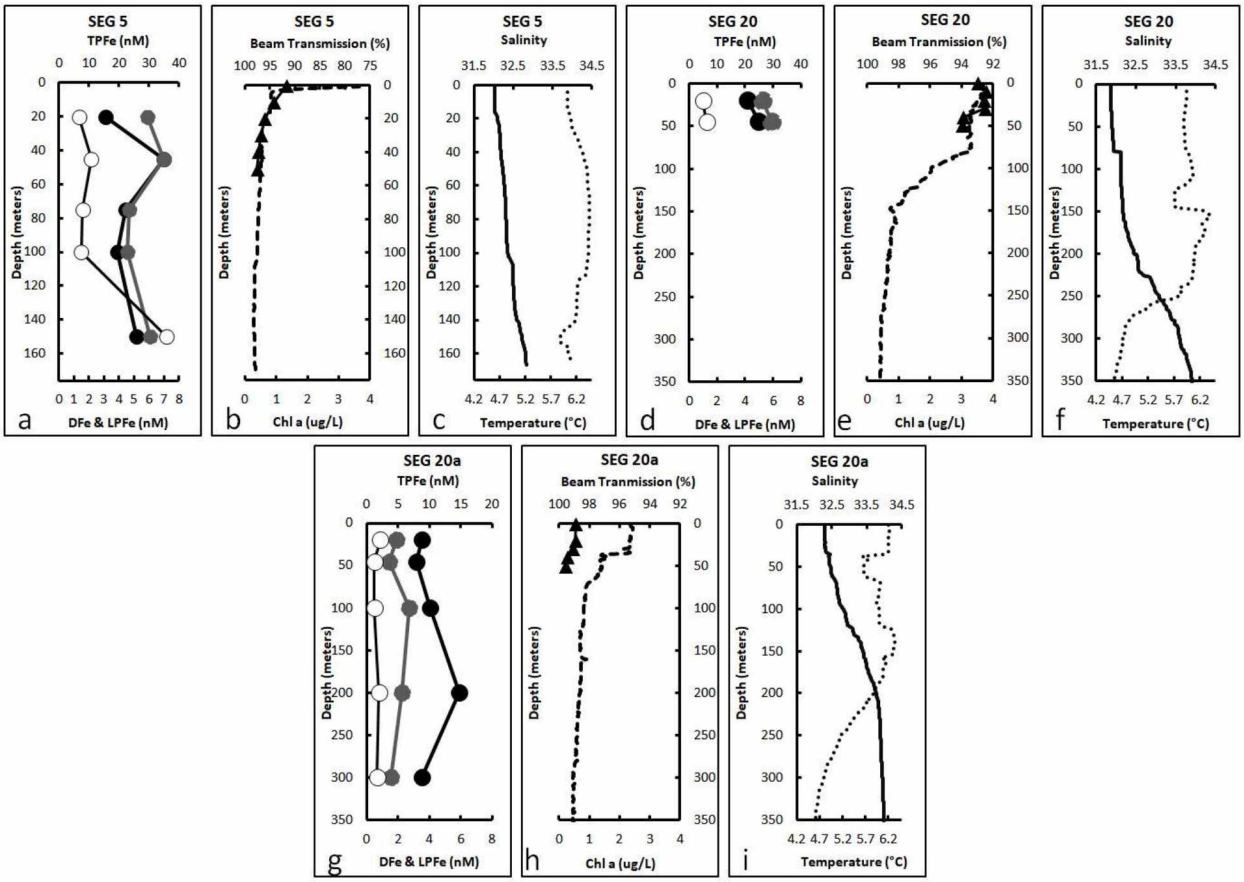

Figure 2.4: Vertical depth profile plots at Stations SEG 5 and SEG 20. Station SEG 20 was sampled twice during the cruise, April 11, 2013 (d, e, f) and April 16, 2013 (g, h, i). DFe (white circles), LPFe (gray circles), TPFe (black circles) (a, d, g) were collected using UAF vanes deployed above the CTD rosette. Beam transmission (%; large dashed line) (b, e, h), salinity (black line) and temperature (dotted line) (c, f,i) were collected from sensors on the ship's CTD rosette. Chlorophyll a (black triangles) (b, e, h) was provided by the Strom Lab.

increased to > 96 % below 10 m. Chlorophyll biomass was 1.34 μg/L at the surface, but decreased from 0.93 μg/L at 10 m to 0.39 μg/L at 50 m. Bottom depths increased from 176 m at Station SEG 5 to 1666 m at Station SEG 20. Station SEG 5 was sampled at 5 depths for Fe species which remained high throughout the water column. The TPFe ranged from 15.5 to 34.9 nM and DFe ranged from 1.3 nM at the surface to a subsurface maximum of 7.2 nM at 150 m. The LPFe fraction was highest at 20 m with 38 % of the TPFe, while at depth it remained between 20 – 23 % of the TPFe. The concentrations of LPFe remained relatively homogenous throughout the water column (4.6 – 7.0 nM). Station SEG 20 was sampled at two depths, but was also reoccupied five days later with samples taken at five depths. During the first

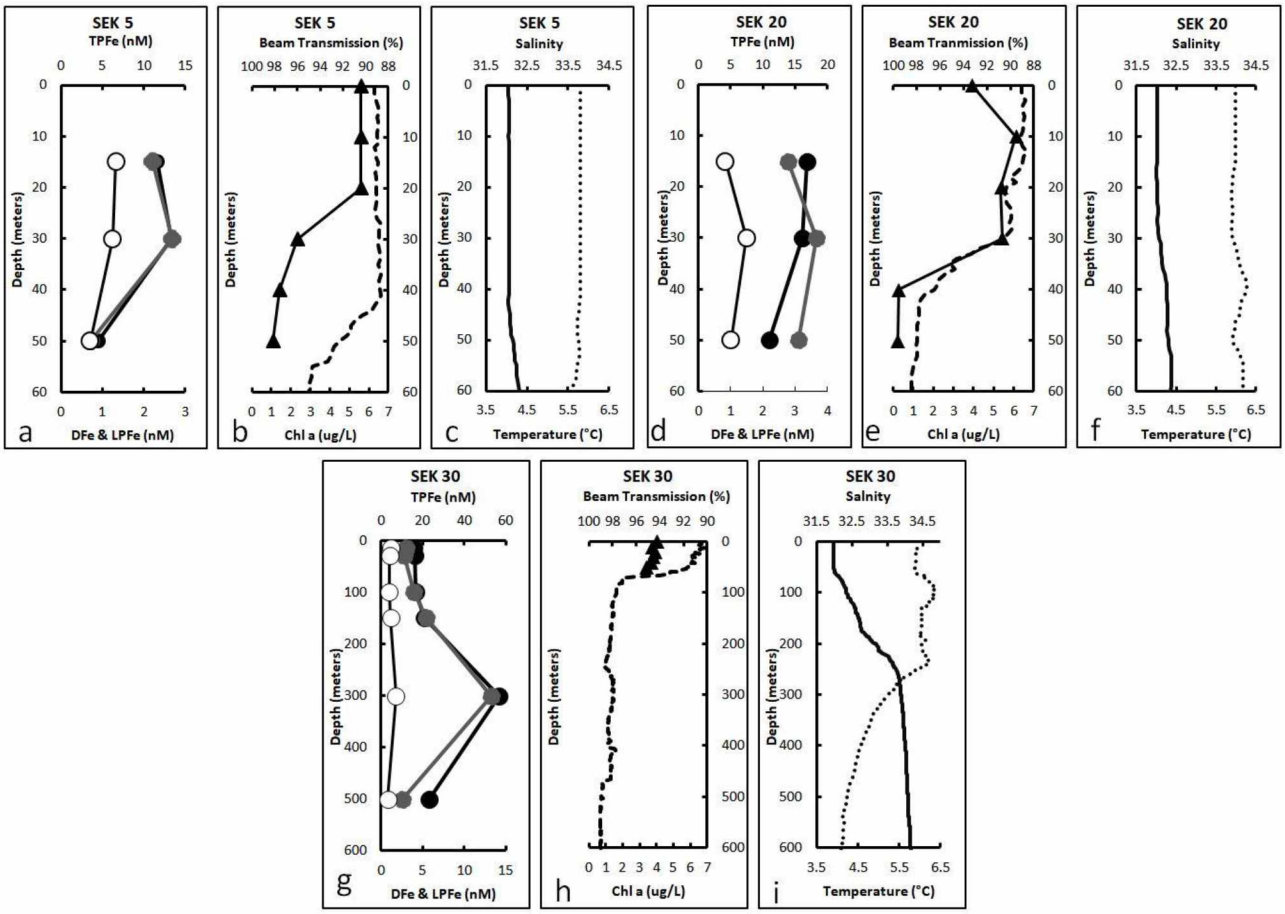

Figure 2.5: Vertical depth profile plots at Stations SEK 5, SEK 20, and SEK 30. DFe (white circles), LPFe (gray circles), TPFe (black circles) (a, d, g) were collected using UAF vanes deployed above the CTD rosette. Beam transmission (%; large dashed line) (b, e, h), salinity (black line) and temperature (dotted line) (c, f, i) were collected from sensors on the ship's CTD rosette. Chlorophyll a (black triangles) (b, e, h) was provided by the Strom Lab.

sampling, the mixed layer depth was much deeper (~ 80 m) than during the later occupation (~ 35 m). The beam transmission was ~ 92 % within the mixed layer during the first occupation but it increased (~ 95 %) by the time of the second occupation. Chlorophyll biomass was greater during the first sampling, ranging 3.0 – 3.7 µg/L within the mixed layer, and decreased during the second sampling (0.2 – 0.6 µg/L). During the initial occupation, TPFe was 21 nM at 20 m and 24.9 nM at 45 m. The LPFe was ~ 24 % of the TPFe at both depths. During the later sampling, the TPFe increased with depth from 8.8 nM at 20 m to 14.8 nM at 200 m, and decreased again to 8.8 nM at 300 m. Lower concentrations of DFe were observed during both occupations, remaining between 0.5 and 0.9 nM. The LPFe fraction ranged from 15 % to 27 % of the TPFe along the profile, with the highest percentage at 100 m depth.

Along Transect SEK, vertical profiles were characterized by increasing amounts of TPFe from the inner shore station to the offshore station (Figure 2.5). The bottom depths at the inner shelf station (SEK 5) was 154 m, mid shelf station (SEK 20) was 224 m, and off shore station (SEK 30) was 2159 m. The mixed layer depth remained relatively constant (~ 45 m) from inner shelf at SEK 5 to off shore at SEK 30 with a salinity of ~ 32. This was matched with reduced beam transmission across the shelf within the mixed layer (~ 88 – 91 %) and increased chlorophyll biomass concentrations between 1.1 – 5.6 μg/L at SEK 5, 0.23 – 6.1 μg/L at SEK 20, and 3.8 – 3.9 μg/L at SEK 30. Below the mixed layer, salinity increased to ~ 33 near the bottom at SEK 5 and up to 34 near the bottom at SEK 20. AT SEK 30, salinity increased to 34 at ~ 240 m. Similar concentrations of DFe were observed at these stations, ranging 0.7 – 1.8 nM. At Stations SEK 5 and SEK 20, samples were collected within or immediately below the mixed layer at 15, 30, and 50 m. At Station SEK 5, TPFe was similar at 15 and 30 m with 11.6 and 13.3 nM respectively but decreased to 4.5 nM at 50 m. The LPFe fraction decreased with depth at SEK 5 with ~ 19 % of the TPFe (2.2 nM) at 15 m to 15 % of the TPFe (0.72 nM) at 50 m. At Station SEK 20, the TPFe decreased from 16.9 nM at 15 m to 11.0 nM at 50 m. Here, the LPFe fraction increased with depth from 17 % of the TPFe at 15 m to 28 % at 50 m. At Station SEK 30, samples were collected between 100 and 500 m in addition to the mixed layer samples. Within the mixed layer, the TPFe was ~ 16 nM but increased to a subsurface maximum of 56.5 nM at 300 m. The TPFe decreased to 23.3 nM at 500 m. The LPFe fraction at Station SEK 30 tracked changes in TPFe, and also exhibited a subsurface maximum at 300 m. The leachable particulate fraction was greater in the top 150 m (19.2 % – 26 % of the TPFe), and least at 500 m (10.8 %). The concentrations of LPFe ranged from 2.8 – 13.3 nM.

2.3.1.3 Vertical profiles: Northern shelf

Depth profiles for DFe, LPFe, TPFe, salinity, temperature, beam transmission, and chlorophyll a for the Northern shelf are shown in Figures 2.6 and 2.7. Over the northern shelf, two Yakutat Bay Transects, YBC and YBE, and two Kayak Island Stations (KIA, KIB) were sampled April 19 – 23, 2013. Transect YBC was sampled ~10, ~30, and ~50 km from shore and Transect YBE was sampled at ~40 km from shore. Surface temperatures in this region ranged from ~ 5.0 °C to 6.4 °C, with the coldest temperature near Yakutat Bay. Surface salinity gradients from inshore to offshore ranged from 31.9 to 32.6. The Yakutat transects are characterized by a broader shelf where bottom depths were 163 m (YBC 10), 145 m (YBC 30), and 206 m (YBC 50). Beam transmission was correlated with Chl a at the surface, but show subsurface attenuation at Stations YBC 10 and YBC 30 (Figure 2.6 b, e). Chlorophyll biomass remained < 1.0 μg/L (range: 0.4 – 0.8 μg/L) at both of these stations. Salinity and temperature increased in bottom waters at all stations (Figure 2.6c, f, i, l). Surface temperature decreased from YBC 10 (~ 6.5°C) to YBC 50 (~ 5.7°C) (Figure 2.6c, f, i, l). The chlorophyll biomass increased with depth at

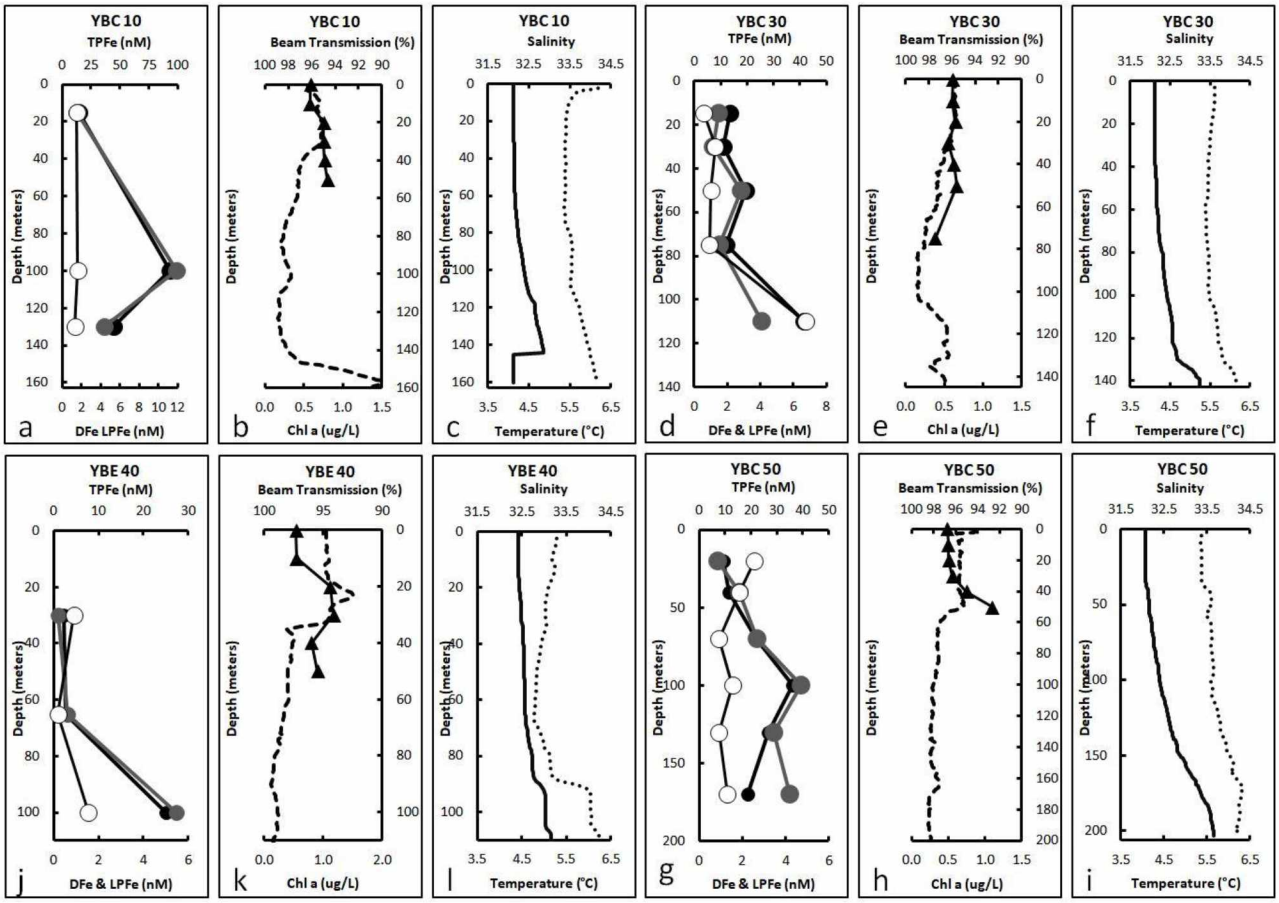

Figure 2.6: Vertical depth profile plots at Stations YBC 10, YBC 30, YBC 50, and YBE 40. DFe (white circles), LPFe (gray circles), TPFe (black circles) (a, d, g, j) were collected using UAF vanes deployed above the CTD rosette. Beam transmission (%; large dashed line) (b, e, h, k), salinity (black line) and temperature (dotted line) (c, f, i, l) were collected from sensors on the ship's CTD rosette. Chlorophyll a (black triangles) (b, e, h, k) was provided by the Strom Lab.

Stations YBC 10, YBC 50, and YBE 40, but showed less variability at Station YBC 30. The trend for all YBC stations was a subsurface maximum in TPFe at ~ 100 m (Figure 2.6a, 2.6d, and 2.6g). At YBC 10, the TPFe ranged 14.6 – 93 nM. The LPFe fraction remained between 9.7 – 12.8 % of the TPFe, while concentrations ranged from 1.6 to 11.9 nM. Dissolved Fe was relatively homogenous throughout the water column ranging between 1.3 – 1.6 nM. At Station YBC 30, the TPFe ranged from 11 nM to 41.6 nM. The LPFe fraction was variable with 9.9 – 14.7 % of the TPFe. The DFe was variable but increased from 0.6 nM at 15 m to a subsurface maximum of 6.8 nM at 110 m. At Station YBC 50, the TPFe was elevated but variable, ranging between 9.4 – 36.1 nM. The LPFe was also elevated but variable, ranging between 9.4 – 22.5 % of the TPFe. The DFe decreased from 2.6 nM at 20 m to 1.3 nM at 170 m. Station YBE 40 was sampled at 30, 65, and 100 m depth for Fe species. The concentrations of TPFe were similar

~ 2.5 nM at 30 and 65m but there was an increase at 100 m to 25.0 nM. The LPFe fraction increased from 8.4 % of the TPFe at 30 m to ~ 22 % at 100 m. The DFe concentrations here ranged from 0.2 – 1.5 nM.

Two stations near Kayak Island, one inner shelf, KIB A, and one over the outer shelf, KIA 4, had bottom depths of 212 m and 1175 m, respectively. Surface temperature and salinity for the KIB A were 5.2°C and 32.0, and these were similar for KIA 4 (5.7°C and 32.4). The water column was relatively well mixed down to 40 m at Station KIB A with salinities increasing up to 33.3 near the bottom. The beam transmission was variable over the water column (88 – 93 %). The mixed layer depth was ~50 m KIA 4 with salinity increasing minimally down to 100 m, but changing more rapidly below this depth. The temperature here decreased from 5.7°C to 4.3°C at 100 m and then increased to maximum temperature of ~6°C at 140 m. The beam transmission and chlorophyll biomass were observed to have a similar trend, where beam transmission slowly increased from ~ 90 % at the surface to 98 % at 60 m and chlorophyll decreased from 2.5 µg/L near the surface to 0.9 µg/L at 50 m. Both Kayak Island stations displayed the same trend with increasing concentrations of suspended particulate Fe with depth, but KIB A exhibited an order of magnitude greater concentrations (see Figure 2.7a and 2.7d). At Station KIB A, the TPFe increased from 493.8 nM at 15 m to 861.2 nM at 110 m. The LPFe fraction was variable ranging from 8.6 % to 14.5 % with a subsurface maximum at 65 m. The samples for DFe were likely contaminated (26.5 – 44.3 nM) so results are not shown here. At Station KIA 4, concentrations of TPFe were low down to 100 m (2.5 – 4.7 nM), but concentrations increased with depth to a maximum of 47.4 nM at 300 m.

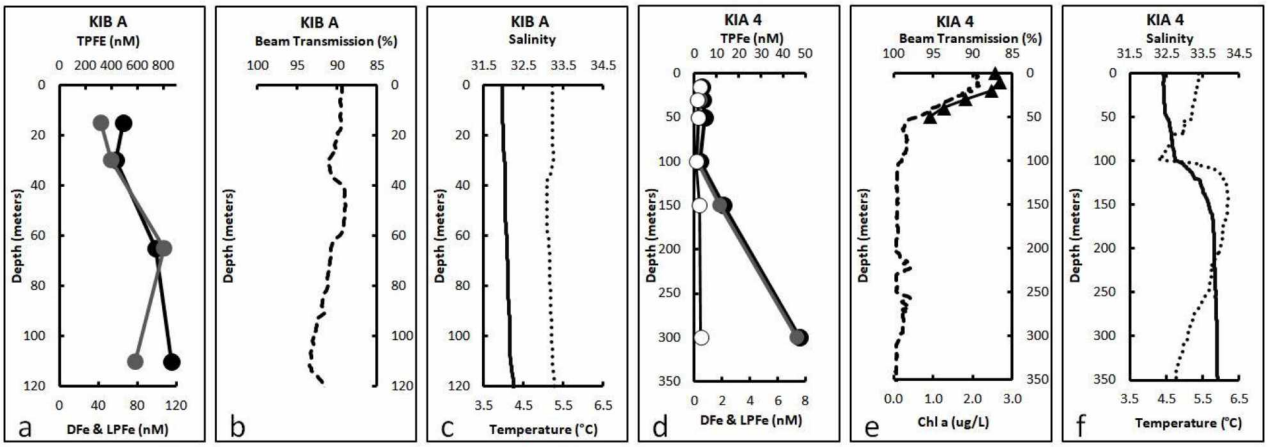

Figure 2.7: Vertical depth profile plots at Stations KIB A and KIA 4. DFe (white circles), LPFe (gray circles), TPFe (black circles) (a, d) were collected using UAF vanes deployed above the CTD rosette. Beam transmission (%; large dashed line) (b, e), salinity (black line) and temperature (dotted line) (c, f) were collected from sensors on the ship's CTD rosette. Chlorophyll a (black triangles) (e) was provided by the Strom Lab.

The LPFe fraction followed a similar trend with percentages decreasing from 11.5 % of the TPFe at 15 m to 5.3 % at 50 m. The percent LPFe increased from 9.8 % of the TPFe at 100 m to 15.6 % at 300 m. The concentrations of LPFe ranged from 0.4 nM at 15 m to 7.4 nM at 300 m. The DFe concentrations were very low and remained between 0.14 – 0.48 nM.

2.3.1.4 Vertical profiles: Western shelf

Depth profiles for DFe, LPFe, TPFe, salinity, temperature, beam transmission, and chlorophyll a for the Western shelf are shown in Figures 2.8 and 2.9. Four stations, 197-HL, 197-HT, 181-HL, and 185-HX, were sampled at transects that ran perpendicular to Kodiak Island between the dates of April 27 – 30, 2013. Two stations along the GAK Line (GAK 1 and GAK13) were sampled between May 3 – 5, 2013. Bottom depths at Stations 197-HL and 197-HT were 80 m and 180 m, respectively. The surface salinity from inner to outer shelf was 32.3 to 32.4, and the same temperature (4.4°C) was observed at both stations. The water column was well mixed at Station 197-HL, and a minimal increase in temperature and salinity were observed near the bottom at Station 197-HT. The beam transmission at Station 197-HL was homogenous throughout the water column at ~ 89 %, while at Station 197-HT it ranged from 90 % in the upper water column and 93 % at depth. The chlorophyll biomass was variable ranging from 3.3 – 3.9 μg/L at Station 197-HL and 2.6 – 3.2 μg/L at Station 197-HT. At Station 197-HL, TPFe concentrations increased with depth from 311.9 nM at 20 m to 352.4 nM at 50 m. The LPFe fraction decreased with depth from 14 % to 6 % of the TPFe. Dissolved Fe was variable ranging from 0.56 – 0.77 nM. At Station 197-HT, the TPFe was lower than at Station 197-HL, and ranged from 194.8 nM to 241.7 nM. In contrast, higher concentrations of DFe were observed. These increased with depth from 0.79 nM at 20 m to 1.1 nM at 150 m. The LPFe fraction was similar down to 75 m (6.6 – 8.1 % of the TPFe), but increased to ~ 22% at 150 m. Water depth at Stations 181-HL and 185-HX were 83 and 2853 m, respectively. Here, small changes in surface salinity and temperature from inner shelf to outer shelf were observed, from 32.4 to 32.7 and 4.9°C to 4.7°C. The bottom depth for 181-HL station was 80 m and was well mixed. The beam transmission increased with depth from ~ 79 % at the surface to ~ 91 % at depth, reflecting changes in Chl a (Figure 2.8h). Samples for Fe species were obtained at 15, 30, 45 and 60 m. Large increase in TPFe with depth from 25.3 nM at 15 m to 222.1 nM at 60 m were observed (Figure 10g). Increase in LPFe with depth were also observed, but the LPFe fraction was highly variable ranging from 9.2 % to 37.3 % of the TPFe. The DFe also increased with depth from 0.69 nM at 15 m to 2.05 nM at 60 m. At Station 185-HX, the mixed layer depth was ~ 35 m. Samples for Fe species were obtained at 15, 30, and 50 m. The beam transmission ranged from 88 % in the upper water column to ~ 98 % at depth. Chlorophyll biomass was

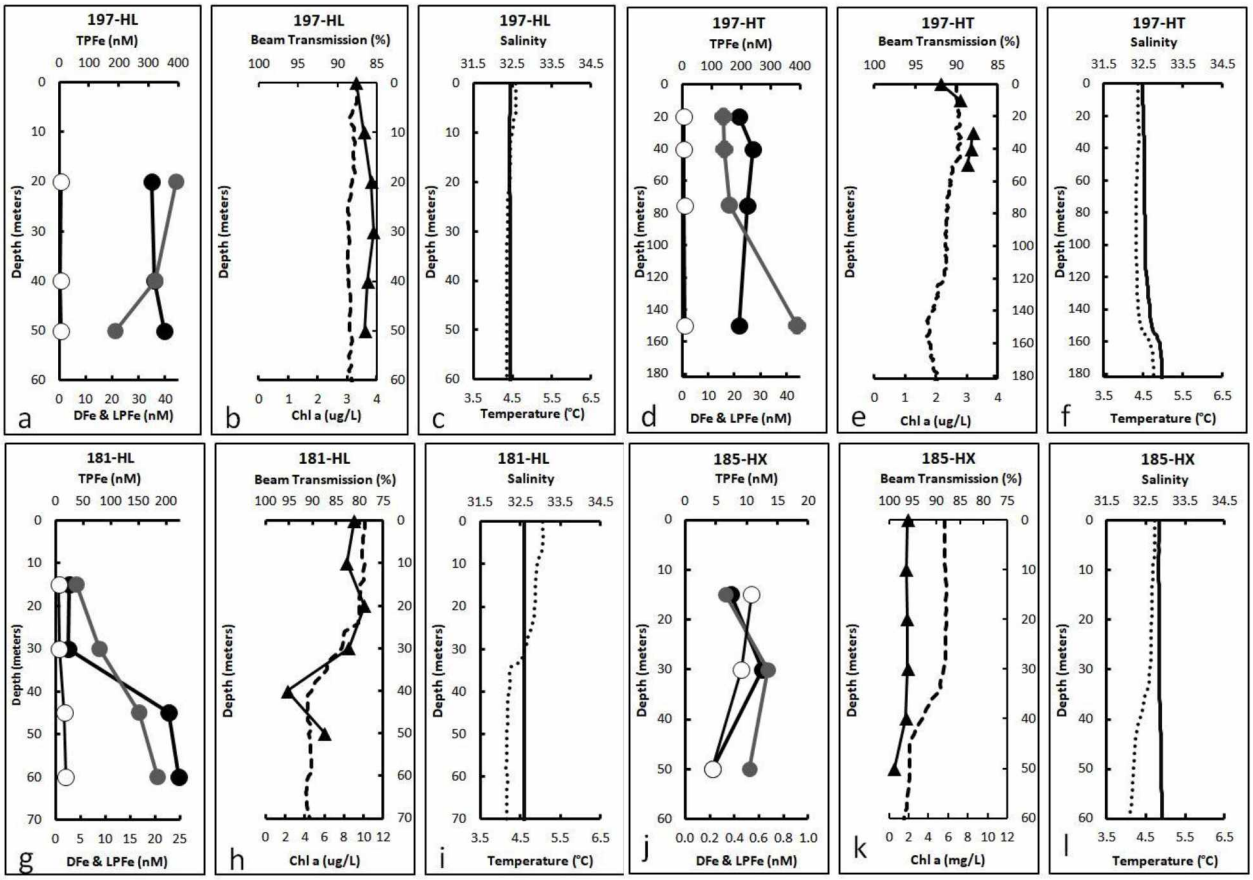

Figure 2.8: Vertical depth profile plots at Stations 197-HL, 197-HT, 181-HL, and 185- HX. DFe (white circles), LPFe (gray circles), TPFe (black circles) (a, d, g, j) were collected using UAF vanes deployed above the CTD rosette. Beam transmission (%; large dashed line) (b, e, h, k), salinity (black line) and temperature (dotted line) (c, f, i, l) were collected from sensors on the ship's CTD rosette. Chlorophyll a (black triangles) (b, e, h, k) was provided by the Strom Lab.

relatively low and varied little with depth decreasing from 1.9 µg/L at the surface to 0.5 µg/L at 50 m. Here, the TPFe was much lower than at other Kodiak region stations ranging between 4.4 – 12.5 nM. The LPFe fraction increased with depth from 4.4 % of the TPFe at 15m to 11.8 % at 50 m. Dissolved Fe decreased down the water column from 0.54 nM at 15 m to 0.22 nM at 50 m.

The inner shelf (GAK 1) and slope (GAK 13) were sampled along the GAK Line. At GAK 1, samples for Fe parameters were collected at 25, 50, 100, and 190 m, while at GAK 13 due to equipment malfunction, samples for Fe parameters were only collected at 80, 110, and 1150 m. At GAK 1 salinity increased from 31.5 at the surface to a maximum of about 33 at 250 m. A warm water lense was observed at the surface, below water temperature decrease to a minimum of 4.5°C at 75 m, from where it again increased with depth to a maximum of 5.5°C at 250 m. Variable % beam transmission in the upper 40 m

reflected changes in Chl a concentrations. The observed reduction in % beam transmission 40 – 70 m did not coincide with increases in Chl a. At mid-depths (75 – 180 m) % beam transmission as high as 95 %, and below it decrease again to a minimum of 90 %. Dissolved Fe increased from 1.0 nM at 25 m to 2.8 nM at 190 m. This increasing trend was also seen in LPFe and TPFe. Here, the fraction of PFe that was leachable varied from 5.3 % to 14.9 %. Station GAK 13 was oceanic in character, with higher salinity (~ 33 – 34), cooler waters (3.75° – 5.0°C) and reduced Chl a values of 1 μg/L. Yet % beam transmission was as low as 86 % in the upper 20 m and increased rapidly below 60 m to a max of 98 % at 250 m. A decrease with depth was observed for TDFe and LPFe, from 80 m to 150 m, while DFe remain constant in the two samples below 100 m. The LPFe fraction varied little from 10 % to 13 % of the TPFe.

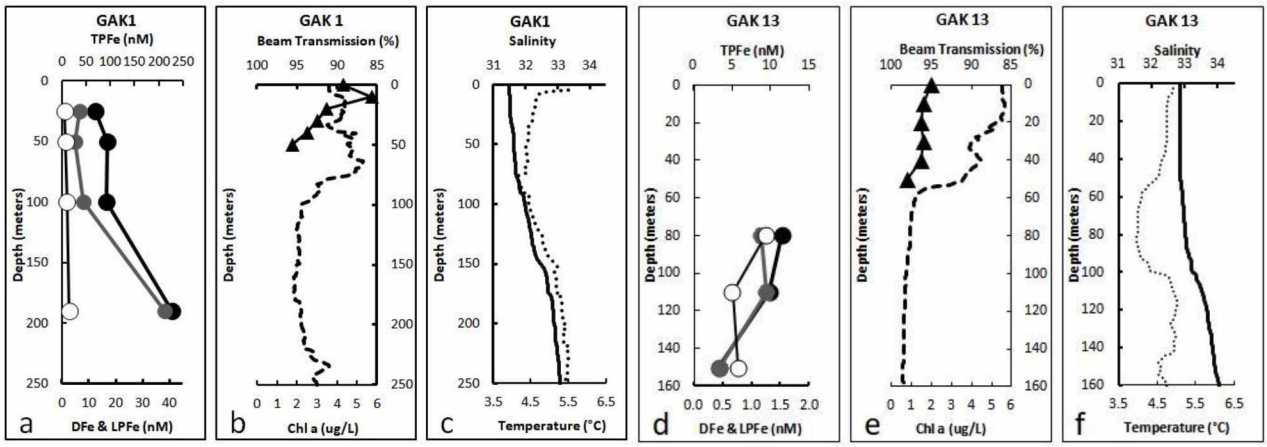

Figure 2.9: Vertical depth profile plots at Stations GAK 1 and GAK 13. DFe (white circles), LPFe (gray circles), TPFe (black circles) (a, d) were collected using UAF vanes deployed above the CTD rosette. Beam transmission (%; large dashed line) (b, e), salinity (black line) and temperature (dotted line) (c, f) were collected from sensors on the ship's CTD rosette. Chlorophyll a (black triangles) (b, e) was provided by the Strom Lab.

2.3.1.5 Surface dissolved and particulate Fe: GAK Line

Surface particles were obtained along the GAK Line (Transect 1TX5). Temperature in surface waters ranged from 4.6 °C at the inner shelf, 5.5 – 6.3°C mid-shelf, and 4.0°C at the outer shelf station (Figure 2.2b). Surface salinities ranged from 31.5 shoreward to 32.3 offshore (GAK 8) (Figure 2.2a). Particulate and dissolved Fe from GAK 3 to GAK 5 generally decreased and then increased further offshore (see Figure 2.10). The range in TPFe was from 96.6 nM (latitude 59.57) to 24.1 nM (latitude 59.26). Here DFe ranged from 0.40 to 2.01 nM. The LPFe fraction was highly variable ranging from 7.1 % to 25.7 % of the TPFe (Figure 2.10).

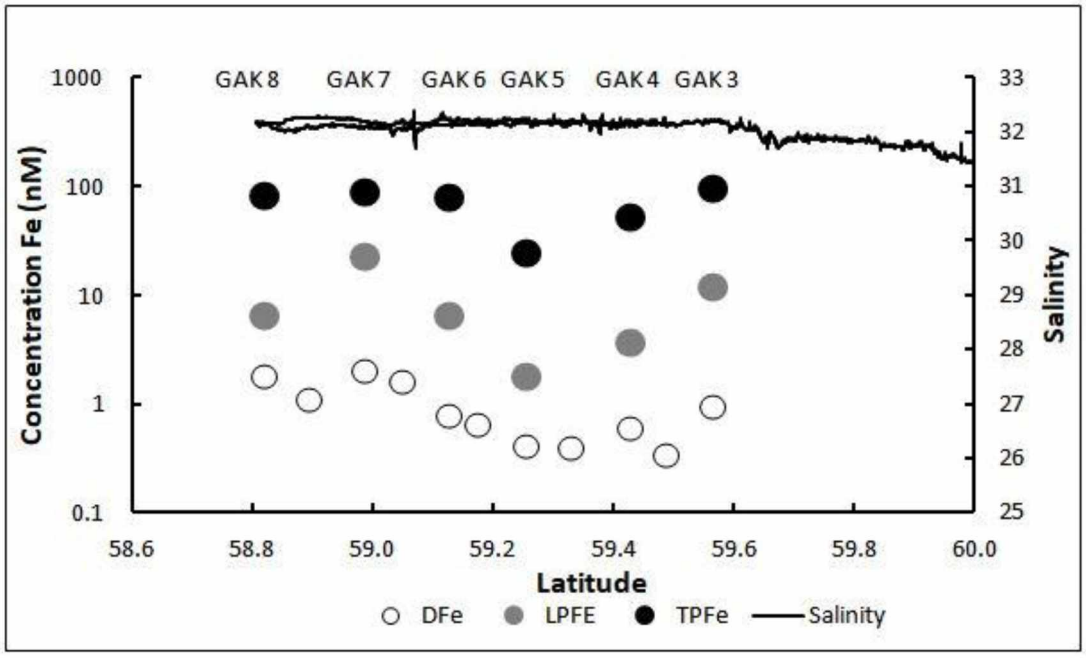

Figure 2.10: Transect plot of the GAK Line in the late spring with the species of Fe (TPFe = black circles, LPFe = gray circles, DFe = white circles) and salinity as a function of latitude (latitude 60.0 is the start of the transect).

2.3.1.6 Vertical profiles: Prince William Sound

During the late spring cruise, a vertical profile near CG in PWS (Figure 2.11) showed cold (3.7°C) and fresh salinity (28.5). Surface waters with low beam transmission (~ 70 %) and concomitant high concentrations of TPFe (1.1 μM) of which LPFe accounted for ~ 14 %. A decreasing trend in TPFe with depth followed the trend in increasing % beam transmission. In contrast, LPFe and DFe had asubsurface maxima at 20 m. Temperature and salinity increased sharply with depth to a maximum of 5.4°C and 32.5 respectively. Although particulate Fe was extremely high at this station (361 nM to 1.1 μM), DFe was relatively constrained ranging from 1.8 nM to 7.6 nM. The LPFe decreased sharply from 279.7 nM at 20 m to 37.8 nM at 100 m.

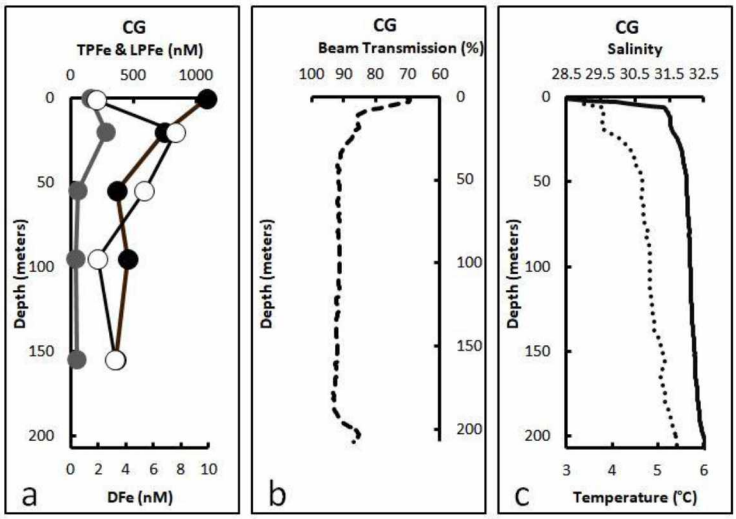

Figure 2.11: Vertical depth profile plots for Station CG. DFe (white circles), LPFe (gray circles), TPFe (black circles) (a) were collected using UAF vanes deployed above the CTD rosette. Beam transmission (%; large dashed line) (b), salinity (black line) and temperature (dotted line) (c) were collected from sensors on the ship's CTD rosette.

2.3.2 Early fall

2.3.2.1 Surface dissolved Fe distributions

Surface salinity, temperature, and DFe for the early fall surface transects are shown in Figure 2.12. Eleven transects were sampled during September 13 – 26, 2013, which spanned a portion of the Western shelf and covered most of the Northern and Southeastern shelves. Over the Southeastern shelf, surface salinity ranged from 30 to 31.5 closer to the coast where the ACC is present and seaward salinities increased (> 32). Low salinities (< 29) were observed over much of the Northern shelf both in and around PWS and at the mouth of Yakutat Bay. Over the Western shelf, salinities were low (< 30) closer to shore at the GAK line but salinities increased quickly to over 32 over the rest of the shelf. Surface water temperature across the shelf was generally warmer (>13°C) along the Southeastern shelf. Near the mouth of Yakutat Bay surface water temperature was ~ 12°C and quickly increased seaward to ~ 14°C. North and west of Yakutat Bay surface waters temperatures were much cooler (< 12°C). The DFe concentrations were generally higher over the Western and Northern shelves. Transects over the Southeastern shelf (2TX1, 2TX2, 2TX3, and 2TX4) were observed to have low DFe, with an average of

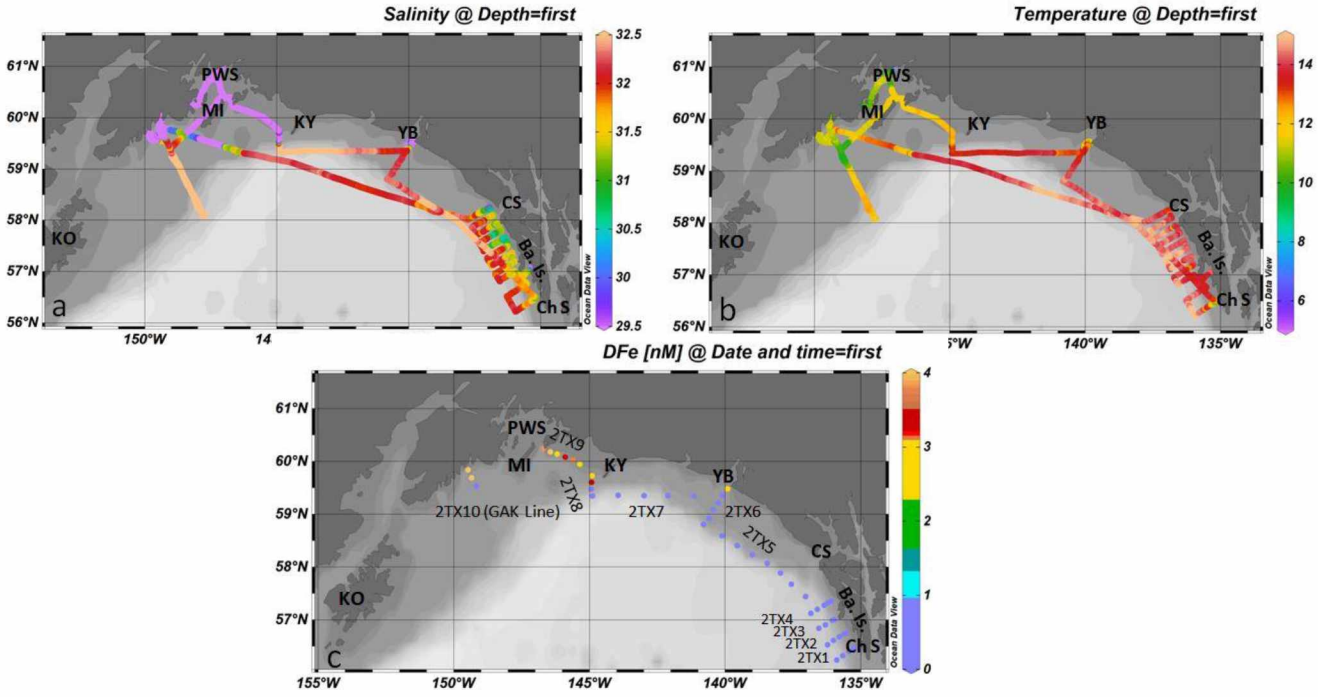

Figure 2.12: Maps of the surface transects during early fall 2013 along the Gulf of Alaska shelf. Salinity (a) and temperature (b) were obtained from the ship's underway system. Samples for the analysis of dissolved Fe (c) obtained from the trace-metal-clean towed system.

0.43 nM. Transitioning to the northern shelf, Transect 2TX5 was located over the outer shelf, and exhibited low concentrations of DFe, with a minimum of 0.14 nM and a maximum of 0.63 nM. Transect 2TX6 extended from the mouth of Yakutat Bay to the shelf. Elevated DFe (2.96 nM) was found closer to the mouth of Yakutat Bay where fresher waters (S = 28.2) were observed but the remaining transect was low in DFe with an average of 0.49 nM. Along Transect 2TX7, DFe exhibited low values with an average of 0.28 nM. Transect 2TX8 ran along 145°W where a significant decrease in salinity from the offshore (~ 32.6) to the mid-shelf (~ 27.9) was observed. Decreases in salinity were accompanied by increases in DFe from 0.26 nM offshore to 3.3 nM over the shelf. West of Kayak Island, the shelf widens, and includes connections with PWS. In this region Transects crossed low salinity colder waters likely influenced by the Copper River and outflow from PWS. Here, Transect 2TX9 and 2TX10 exhibited higher DFe concentrations (~ 2.7 to 4.1 nM).

2.3.2.2 Surface dissolved and particulate Fe: GAK Line

During fall (September 24 – 26), the GAK Line (Transect 2TX10) was sampled for surface particles at odd numbered stations (GAK 1 through GAK 13). Here, temperatures ranged from 10.8°C near shore, 9.8°C mid shelf, and 12.2 – 11.3°C for outer shelf (Figure 2.12b). The salinity was 25.9 in the

near shore ACC, 32 – 32.3 in the mid shelf, and 32.5 in the outer shelf. Particulate Fe exhibited variable cross-shelf concentrations (Figure 2.13). The highest concentration (218.8 nM TPFe) was observed within ACC waters, while it decreased from GAK 3 to GAK 7 from 52.1 nM to 21.7 nM. Seaward of GAK 7, increases in TPFe were observed from 46.0 to 134.3 nM. The LPFe fraction was generally low (~ 3 % of TPFe), but variable in concentration ranging from 0.18 to 8.7 nM. As noted above, DFe was elevated within the ACC, 5.8 and 5.4 nM, but decreased sharply (0.86 nM) at GAK 3 in more saline waters (S ~ 32).

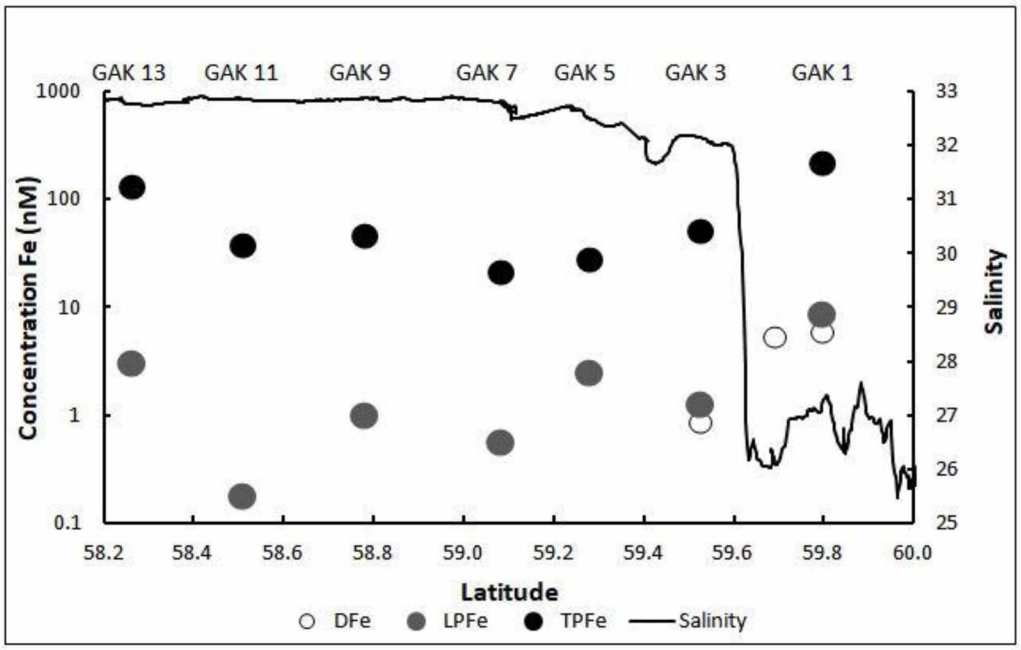

Figure 2.13: Transect plot of the GAK Line in early fall 2013, with the various species of Fe (TPFe = black circles, LPFe = gray circles, DFe = white circles) and salinity as a function of latitude (60°N is the inshore side of the transect). Note the order of magnitude changes in Fe concentrations.

2.3.2.3 Surface dissolved and particulate Fe: Prince William Sound

During fall, waters in CB were sampled at the surface on September 21, 2013. The temperature was 7°C and salinity was 25.9. The surface sample had an extremely high particulate load with 4.8 µM for TPFe. The LPFe accounted for ~ 10 % of the TPFe with 479.2 nM.

2.4 Discussion

2.4.1 Fresh water influence

Freshwater input into the GOA averages 870 $km^3 yr^{-1}$ (Neal et al., 2010) and is mainly trapped within the ACC (Royer, 1987). During the high season (June to November) the GOA receives approximately twice the amount of runoff than it does during the low season (December to May) as a result of increased precipitation and the release of glacial and snow melt (Royer, 1987 Neal et al., 2010). Spatial gradients in freshwater input are due in part to enhanced precipitation in the region southeast of Kayak Island. The enhanced precipitation is brought about by atmospheric circulation patterns that produce intense low-pressure systems in that area, and this disproportionately large amount of rainfall represents ~ 66% of the annual runoff into the GOA (Neal et al., 2010). In contrast, the runoff into the Western GOA accounts for only a fraction of the freshwater discharge (~ 17 %; Neal et al., 2010). The seasonal runoff creates a low salinity core on the shoreward side of the ACC which is observed along the inner GOA shelf although spring salinities in the core are higher than in fall (Stabeno et al., 2004). A distinct elevated Fe signal within these lower salinity waters has been observed from spring through fall (Wu et al., 2009; Lippiatt et al., 2010; Aguilar-Islas et al., 2016). We also observed elevated DFe during the late spring within relatively fresher waters ($S < 31.7$) over the Southeastern shelf and slope, near the mouth of Yakutat Bay, and along much of the wider Western shelf, which is downstream along the surface circulation patterns (Figure 2.2). Over the Southeast shelf, the ACC is less defined but the average flow is northward (Stabeno et al., 2016a). Here, the ACC starts at the southern end of Baranoff Island and continues uninterrupted to Cross Sound encompassing both the shelf and slope system (Stabeno et al., 2016a). Along the coastline are many fjords and inlets that provide avenues for tidal steering and result in complex mixing that directs the transport of freshwater at the inner and mid-shelves (Stabeno et al., 2016a). For example, the waters exiting Chatham Strait flow out and around the southern tip of Baranoff Island and extend out onto the shelf (Stabeno et al., 2016a). Waters exiting the straight can introduce Fe to the surface waters at the Southern tip of Baranoff Island and are a likely source of the lower salinity (~ 31.6), high DFe waters (2.02 – 2.64 nM) observed along Transect DY1 (Figure 2.2). Over this narrow shelf, elevated DFe (1.74 – 2.13 nM) was observed further offshore along Transect DY2 in waters downstream of Chatham Strait (Figure 2.2).

Variable glacial coverage along the coastal mountains also contributes to the spatial variability in fresh water input (Neal et al., 2010). Although glaciers are most abundant along the Northern shelf region (Neal et al., 2010), this glacial input is transported nearshore via the ACC towards the Western region (Stabeno et al., 2004). During the high flow season, glacially influenced rivers and streams carry large loads of suspended particles rich in Fe (Schroth et al., 2011) that alter the character of the ACC, but do

not persist further offshore. This input produces cross-shelf gradients in suspended particulate Fe that expand orders of magnitude in concentration (e.g., Lippiatt et al., 2010), but also vary with seasons. Our sampling in PWS near Columbia Glacier showed a four-fold increase in TPFe from spring (1.1 μM) to early fall (4.8 μM). Yet, TPFe concentrations were an order of magnitude lower (~ 200 nM) at GAK 1 and two orders of magnitude lower at GAK 13 (~ 10 nM) in early fall (Figure 2.13). GAK 1 is located within the ACC in an area influenced by the outflow from PWS (Stableno et al., 2016b), while GAK 13 is located over the continental margin, and not influenced by the ACC. Suspended particles from GAK 13 are likely mainly of biological origin. Gradients in LPFe and DFe were also observed with seasons and across the shelf. Another salient example is the region around Kayak Island, where waters influenced by the Copper River plume (Station KIB, Figure 2.7) exhibited much higher concentrations of all Fe species than waters outside this influence (Station KIA, Figure 2.7).

2.4.2 Other factors that contribute to Fe variability in surface shelf waters

In spring and summer, complex mixing over the GOA shelf is further complicated by episodic coastal downwelling-relaxation and/or upwelling conditions (Stabeno et al., 2016a), which provide opportunity for the offshore transport of surface shelf waters. Coastal upwelling indices for the study region (NOAA/PFEL) show geographical differences in the strength and duration of upwelling/downwelling events during the 2013 sampling periods (Figure 2.14). The upwelling index derived from the location (57°N, 137°W) within the Southeast region indicates this region experienced more intense events compared to the Northern region (upwelling index derived at 60°N, 139°W). Intense events preceding sampling are likely important contributors to the observed variability in water column parameters within the upper 50 – 100 m at any given location and could lead to substantial changes in Fe concentrations in timescales of days, as was observed during the two occupations of Station SEG 20 (Figure 2.4). Concentrations of DFe, LPFe, and TPFe in the upper 50 m decreased approximately two-fold between April 11 and April 16 at SEG 20, reflecting changes in temperature and salinity, and reduction in suspended particles as indicated by Chl a values and bream transmission (Figure 2.4).

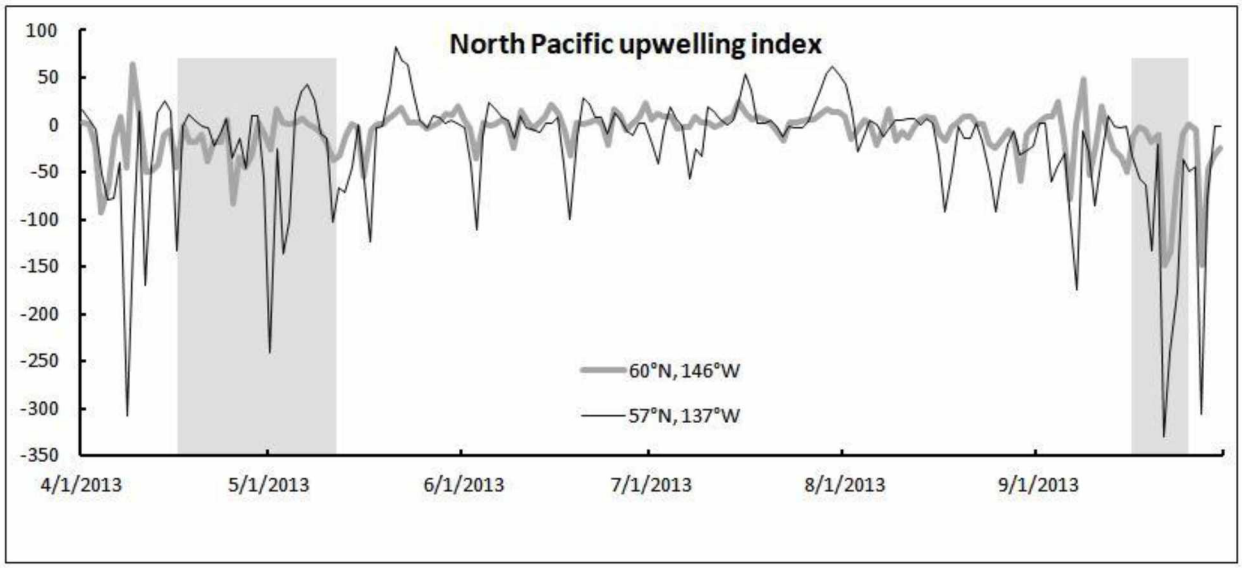

Figure 2.14 North Pacific upwelling index for two stations along the Gulf of Alaska monitored by NOAA's Pacific Fisheries Environmental Laboratory (NOAA/PFEL). Highlighted in gray are the dates of sampling at SEG 20 near the monitored station (57°N and 137°W).

2.4.3 Temporal and spatial variability in reactive Fe

The leachable fraction of suspended particulate Fe can be readily solubilized and become available for biological uptake in a timescale of days (e.g. Hurst and Bruland, 2007). As such, LPFe along with DFe (reactive Fe) are biologically relevant Fe parameters to consider. The large amount of glacially derived suspended particles delivered to the coastal GOA via river plumes results in LPFe becoming the dominant fraction of the reactive Fe pool in surface waters (Lippiatt et al., 2010). The importance of LPFe to the reactive Fe pool decreases with distance from the river plume source and varies with seasons (Aguilar-Islas et al., 2016). During spring, when river discharge is low, DFe can represent a significant portion of the reactive Fe pool. We observed relatively elevated DFe within the mixed layer over the Southeastern shelf in spring 2013 that accounted for between ~18 – 37% of the reactive Fe pool. This range is comparable to that observed during the spring of 2011 (~ 24 – 41%; Aguilar-Islas et al., 2016) in the same region, despite 2011 having below average spring bloom conditions and riverine discharge at the time of sampling. This suggests that the partitioning of reactive Fe during spring is likely mainly influenced by deep winter mixing and the availability of Fe-binding ligands that keep Fe in solution, and less so by the magnitude and timing of fresh water input and the spring bloom. In contrast, during late summer, when river discharge is near its peak, the partitioning of reactive Fe in surface waters of the Northern and Western shelves tends to be dominated by the LPFe fraction with DFe accounting for less than 10 % in low salinity (< 32) waters (Lippiatt et al, 2010; Aguilar-Islas et al., 2016). However, during

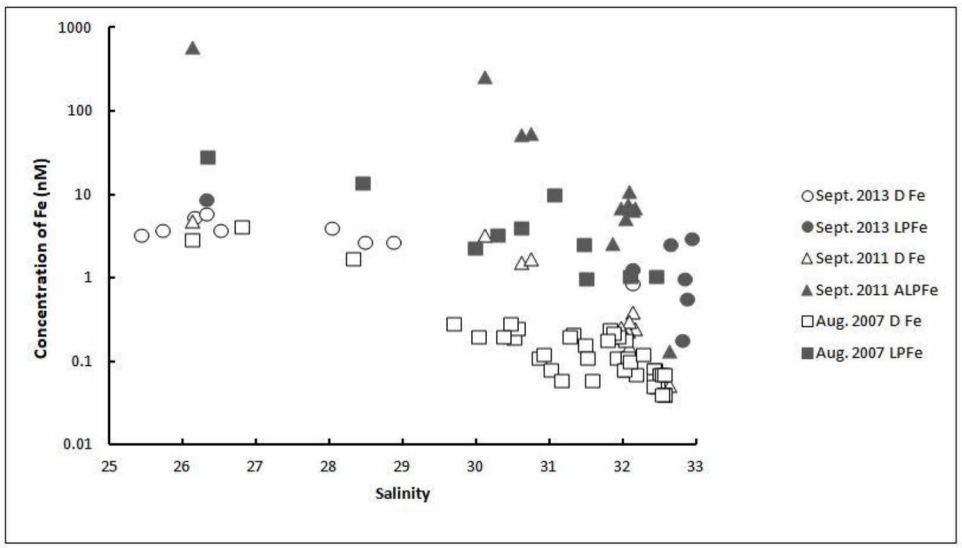

Figure 2.15 Scatter plot of reactive Fe (LPFe & DFe) as a function of salinity along the GAK Line. Note: Sept. 2011 data ("ALPFe") includes all acid labile species where filtered water samples were spiked with a strong acid that might liberate additional Fe species than that of samples processed using a weak acid leach.

fall 2013 the partitioning at GAK 1 and GAK 3 was similar to that observed in spring (~ 40 %) although these surface waters were also relatively fresh (< 32). In general during all sampled years the contribution of DFe to the reactive Fe fraction increases with increasing salinity (Figure 2.15).

2.4.4 Suspended particles characteristics

Aluminum in suspended particles can be used as a tracer of lithogenic material because it is a major component of the Earth's crust, and unlike Fe, it does not have a biological function nor does it undergo phase transition via redox chemistry. Deviations from continental crust Fe/Al ratios (0.40 – 0.63 mass ratio; Clarke and Washington, 1924; Wedepohl, 1995; Rudnick and Gao, 2003; Hawkesworth and Kemp, 2006) of suspended particles can yield insight into oceanographic processes that affect Fe cycling, such as sediment resuspension and lateral advection of the resuspended material, vertical export of biogenic material, and sorption of Fe onto settling particles. The inclusion of biogenic material increases the Fe/Al ratios of suspended sediment because of the minor concentration of Al in biological tissue. The TPFe/TPAl mass ratio of suspended particles from our vertical profiles (0.66) (Figure 2.16) is higher than the upper range of reported ratios for continental crust, suggesting a combination of lithogenic and biogenic particles. The much higher ratio in the leachable particulate fraction (1.86) in our samples suggest the material in this fraction was mainly composed of biogenic material, while the ratio in the refractory fraction (0.58) falls within the range for continental crust. Our ratios are similar to those obtained by a previous study of suspended particles over the Northern shelf of the GOA (Feely et al.,

1981), which found Fe/Al mass ratios ranging from 0.61 for alumino-silicate clays, 0.65 for a mixture of lithogenic and biogenic matter, 2.6 for biogenic matter and 0.65 for suspended particles that were 5 meters from the shelf floor. During our study, areas heavily influenced by glacial input(see circled data points Figure 2.16) exhibited Fe enrichment (Copper River influence at KIB A) or Fe depletion (Columbia Glacier influence) relative to the dominat trend in TPFe/TPAl and RPFe/RPAl ratios, suggesting that processes within Prince William Sound, and the Copper River Plume alter Fe cycling differently from processes occuring over the rest of the shelf. Over the sampled domain, TPFe/TPAl ratios of suspended particles were consistent with the bulk of TPFe having a terrestial source, which had a relatively consistent ratio. A mainly lithogenic source of suspended sediment is similar to what has been observed in other high latitude shelf system, such as the Celtic Sea (Milne et al., 2017).

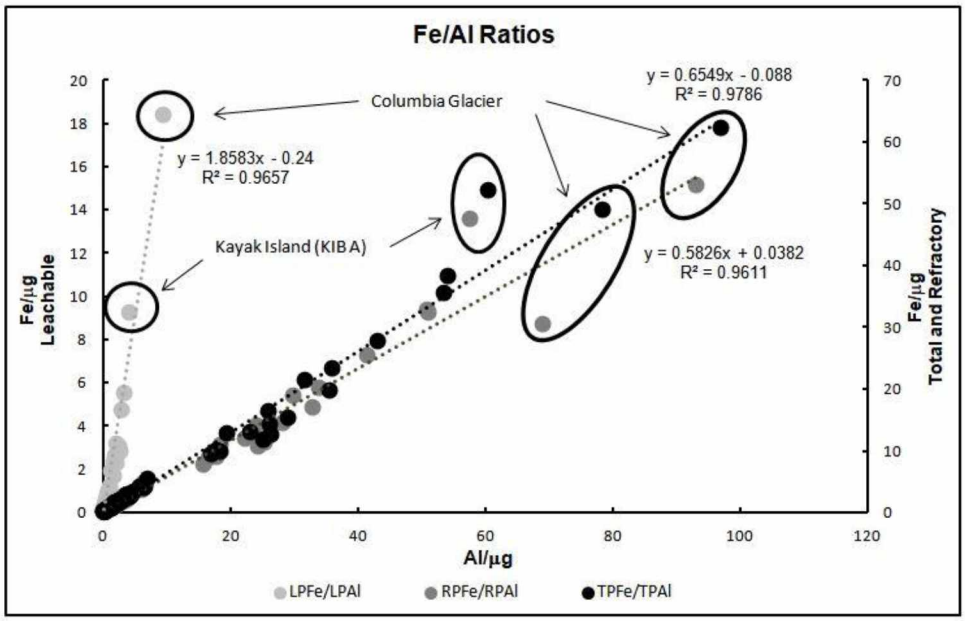

Figure 2.16 Suspended particle Fe/Al ratios for all of the vertical depth profile samples.

2.5 Conclusions

The ACC transports DFe along much of the inner GOA shelf during the late spring and is enhanced by the increase of fresh water input through summer and early fall. Glacial input creates cross shelf gradients for TPFe in the Northern and Western shelves across both sampled seasons. We observed a decreased contribution of the LPFe to the reactive Fe pool in spring from that which has been previously reported for the late summer (Lippiatt et al., 2010), confirming observations made during spring 2011 by Aguilar-Islas et al. (2016). This difference in the contribution of LPFe is likely due to the seasonal cycle of fresh water input, which peaks in late summer/early fall providing a large influx of LPFe. Over the

GOA shelf, complex mixing, bathymetric steering, mesoscale eddies, glacier river plumes, and upwelling/downwelling dynamics have a measurable influence on Fe species throughout the water column, as exemplified by the variability in the magnitude and relative contribution of DFe, LPFe, and RPFe observed across seasons and space in this and previous studies. Across the study region, the main source of suspended particulate Fe is from lithogenic origin. Future Fe work in the GOA should take into account seasonal and spatial variability in fresh water input, vertical mixing and advective features to better understand how the availability of this micronutrient affects production in the GOA.

2.6 Acknowledgements

We thank the captains and crew of the *Oscar Dyson* and *R/V Tiglax* for their assistance on this research. We thank Dr. Marie Seguret for collecting samples and processing them onboard, and for DFe analysis. We thank the Strom Lab (Western Washington University) for collecting, analyzing, and providing the chlorophyll biomass data. This work was supported by funding from the North Pacific Research Board (G84/F4185-00).

2.7 References

Aguilar-Islas, A. M., and K. W. Bruland. 2006. Dissolved manganese and silicic acid in the Columbia River plume: A major source to the California current and coastal waters off Washington and Oregon. Mar. Chem. 101: 233–247.

Aguilar-Islas, A. M., R. Rember, S. Nishino, T. Kikuchi, and M. Itoh. 2013. Partitioning and lateral transport of iron to the Canada Basin. Polar Sci. **7**: 82–99. doi:10.1016/j.polar.2012.11.001

Aguilar-Islas, A. M., M. J. M. Seguret, R. Rember, K. N. Buck, P. Proctor, C. W. Mordy, and N. B. Kachel. 2016. Temporal variability of reactive iron over the Gulf of Alaska shelf. Deep. Res. Part II Top. Stud. Oceanogr. 132: 90–106.

Bell, J., J. Betts, and E. Boyle. 2002. Mitess: A moored in situ trace element serial sampler for deep-sea moorings. Deep. Res. Part I Oceanogr. Res. Pap. 49: 2103–2118.

Berger, C. J. M., S. M. Lippiatt, M. G. Lawrence, and K. W. Bruland. 2008. Application of a chemical leach technique for estimating labile particulate aluminum, iron, and manganese in the Columbia River plume and coastal waters off Oregon and Washington. J. Geophys. Res. **113**: C00B01. doi:10.1029/2007JC004703

Boyd, P. W., C. S. Law, C. S. Wong, and others. 2004. The decline and fate of an iron-induced subarctic phytoplankton bloom. Nature **428**: 549–553. doi:10.1029/2001JB001129

Brown, M. T., S. M. Lippiatt, M. C. Lohan, and K. W. Bruland. 2012. Trace metal distributions within a Sitka eddy in the northern Gulf of Alaska. Limnol. Ocean. **57**: 503–518. doi:10.4319/lo.2012.57.2.0503

Bruland, K.W., Rue, E.L., Smith, G.J., DiTullio, G.R., 2005. Iron, macronutrients and diatom blooms in the Peru upwelling regime: brown and blue waters of Peru. Mar. Chem. 93, 81–103.

Clarke, F. W., and H. S. Washington. 1924. The composition of the Earth's crust. United States Geol. Surv.

Childers, A. R., T. E. Whitledge, and D. A. Stockwell. 2005. Seasonal and interannual variability in the distribution of nutrients and chlorophyll a across the Gulf of Alaska shelf: 1998-2000. Deep. Res. Part II Top. Stud. Oceanogr. **52**: 193–216. doi:10.1016/j.dsr2.2004.09.018

Crusius, J., A. W. Schroth, S. Gassó, C. M. Moy, R. C. Levy, and M. Gatica. 2011. Glacial flour dust storms in the Gulf of Alaska : Hydrologic and meteorological controls and their importance as a source of bioavailable iron. Geophys. Res. Lett. **38**: 1–5. doi:10.1029/2010GL046573

Feely, R. A., G. L. Massoth, and W. M. Landing. 1981. Major- and trace-element composition of suspended matter in the north-east gulf of alaska: relationships with major sources*. Mar. Chem. 431–453.

Hawkesworth, C. J., and A. I. S. Kemp. 2006. Evolution of the continental crust. Nature 443: 811–817.

Hill, D. F., N. Bruhis, C. S.E., A. A. Arendt, and J. Beamer. 2015. Spatial and temporal variability of freshwater discharge into the Gulf of Alaska. J. Geophys. Res. Ocean. 634–646. doi:10.1002/2014JC010395

Hurst, M.P. and K.W. Bruland. 2007. An investigation into the exchange of iron and zinc between soluble, colloidal, and particulate size-fractions in shelf waters using low-abundance isotopes as tracers in shipboard incubation experiments. Mar. Chem. 103: 211-226.

Ladd, C., W. R. Crawford, C. E. Harpold, W. K. Johnson, N. B. Kachel, P. J. Stabeno, and F. Whitney. 2009. A synoptic survey of young mesoscale eddies in the Eastern Gulf of Alaska. Deep Sea Res. Part II Top. Stud. Oceanogr. **56**: 2460–2473. doi:10.1016/j.dsr2.2009.02.007

Lagerström, M. E., M. P. Field, M. Séguret, L. Fischer, S. Hann, and R. M. Sherrell. 2013. Automated on-line fl ow-injection ICP-MS determination of trace metals (Mn, Fe, Co, Ni, Cu and Zn) in open ocean seawater : Application to the GEOTRACES program. Mar. Chem. **155**: 71–80. doi:10.1016/j.marchem.2013.06.001

Lam, P. J., J. K. B. Bishop, C. C. Henning, M. A. Marcus, G. A.Waychunas, and I. Y. Fung. 2006. Wintertime phytoplankton bloom in the subarctic Pacific supported by continental margin iron, Global Biogeochem. Cycles, 20, GB1006, doi:10.1029/2005GB002557.

Lippiatt, S. M., M. C. Lohan, and K. W. Bruland. 2010. The distribution of reactive iron in northern Gulf of Alaska coastal waters. Mar. Chem. **121**: 187–199. doi:10.1016/j.marchem.2010.04.007

Lippiatt, S. M., M. T. Brown, M. C. Lohan, and K. W. Bruland. 2011. Reactive iron delivery to the Gulf of Alaska via a Kenai eddy. Deep. Res. Part I **58**: 1091–1102. doi:10.1016/j.dsr.2011.08.005

Martin, J. H., R. M. Gordon, S. Fitzwater, and W. W. Broenkow. 1989. Vertex: phytoplankton/iron studies in the Gulf of Alaska. Deep Sea Res. Part A. Oceanogr. Res. Pap. **36**: 649–680. doi:10.1016/0198-0149(89)90144-1.

Mote, P. W., E. A. Parson, A. F. Hamlet, and others. 2003. Forests of the Pacific Northwest. Clim. Change **61**: 45–88.

Milne, A., C. Schlosser, B. D. Wake, E. P. Achterberg, R. Chance, A. R. Baker, A. Forryan, and M. C. Lohan. 2017. Particulate phases are key in controlling dissolved iron concentrations in the (sub)tropical North Atlantic. Geophys. Res. Lett. 44: 2377–2387.

Neal, E. G., E. Hood, and K. Smikrud. 2010. Contribution of glacier runoff to freshwater discharge into the Gulf of Alaska. Geophys. Res. Lett. **37**: 1–5. doi:10.1029/2010GL042385

Royer, T. C. 1987. Coastal fresh water discharge in the northeast Pacific. **87**: 2017–2021.

Rudnick, R. L., and S. Gao. 2003. 3.01 - Composition of the Continental Crust. Treatise on Geochemistry 1: 1–64.

Schroth, A. W., J. Crusius, F. Chever, B. C. Bostick, and O. J. Rouxel. 2011. Glacial influence on the geochemistry of riverine iron fluxes to the Gulf of Alaska and effects of deglacation. Geophys. Res. Lett. **38**: 1–6. doi:10.1029/2011GL048367

Stabeno, P. J., N. A. Bond, A. J. Hermann, N. B. Kachel, C. W. Mordy, and J. E. Overland. 2004. Meteorology and oceanography of the Northern Gulf of Alaska. Cont. Shelf Res. **24**: 859–897. doi:10.1016/j.csr.2004.02.007

Stabeno, P. J., N. A. Bond, N. B. Kachel, C. Ladd, C. W. Mordy, and S. L. Strom. 2016a. Southeast Alaskan shelf from southern tip of Baranof Island to Kayak Island: Currents, mixing and chlorophyll-a. Deep. Res. Part II Top. Stud. Oceanogr. **132**: 6–23. doi:10.1016/j.dsr2.2015.06.018

Stabeno, P. J., S. Bell, W. Cheng, S. Danielson, N. B. Kachel, and C. W. Mordy. 2016b. Long-term observations of Alaska Coastal Current in the northern Gulf of Alaska. Deep. Res. II. **132**: 24–40. doi:10.1016/j.dsr2.2015.12.016

Strom, S. L., M. B. Olson, E. L. Macri, and C. W. Mordy. 2007. Cross-shelf gradients in phytoplankton community structure, nutrient utilization, and growth rate in the coastal Gulf of Alaska. Mar. Ecol. Ser. **328**: 75–92. doi:Doi 10.3354/Meps328075

Strom, S. L., K. A. Fredrickson, and K. J. Bright. 2016. Deep-Sea Research II Spring phytoplankton in the eastern coastal Gulf of Alaska : Photosynthesis and production during high and low bloom years. Deep. Res. Part II **132**: 107–121. doi:10.1016/j.dsr2.2015.05.003

Wedepohl, K. H. 1995. The composition of the continental crust. Geochim. Cosmochim. Acta 59: 1217–1232.

Wu, J. 2007. Determination of picomolar iron in seawater by double $Mg(OH)_2$ precipitation isotope dilution high-resolution ICPMS. Mar. Chem. 103: 370–381.

Wu, J., A. Aguilar-Islas, R. Rember, T. Weingartner, S. Danielson, and T. Whitledge. 2009. Size-fractionated iron distribution on the northern Gulf of Alaska. Geophys. Res. Lett. **36**: 1–4. doi:10.1029/2009GL038304

2.8 Appendices

APPENDIX A: Surface transects iron data for Cruise DY in the late spring 2013.

Cruise	Transect	Date	Longitude [degrees_east]	Latitude [degrees_north]	Depth [m]	DFe [nM]	LPFe[nM]	RPFe[nM]	TPFe[nM]
DY	DY1	4/14/2013	-134.68	56.14	Surface	2.64			
DY	DY1	4/15/2013	-134.57	56.15	Surface	2.02			
DY	DY1	4/15/2013	-134.46	56.16	Surface	2.18			
DY	DY1	4/15/2013	-134.38	56.17	Surface	2.46			
DY	DY2	4/16/2013	-135.96	56.57	Surface	1.74			
DY	DY2	4/16/2013	-136.02	56.63	Surface	1.74			
DY	DY2	4/16/2013	-136.08	56.69	Surface	2.13			
DY	DY2	4/16/2013	-136.14	56.75	Surface	1.67			
DY	DY3	4/18/2013	-137.68	58.12	Surface	1.14			
DY	DY3	4/18/2013	-137.85	58.15	Surface	1.04			
DY	DY3	4/18/2013	-138.06	58.18	Surface	1.14			
DY	DY3	4/18/2013	-138.21	58.20	Surface	1.12			
DY	DY3	4/18/2013	-138.36	58.23	Surface	1.13			
DY	DY3	4/18/2013	-138.48	58.24	Surface	0.84			
DY	DY3	4/18/2013	-138.61	58.26	Surface	0.79			
DY	DY3	4/18/2013	-138.69	58.28	Surface	0.91			
DY	DY4	4/18/2013	-139.19	58.64	Surface	0.79			
DY	DY4	4/18/2013	-139.22	58.71	Surface	0.76			
DY	DY4	4/18/2013	-139.26	58.78	Surface	0.74			
DY	DY4	4/18/2013	-139.32	58.87	Surface	0.75			
DY	DY4	4/18/2013	-139.37	58.95	Surface	0.98			
DY	DY4	4/18/2013	-139.41	59.02	Surface	0.38			
DY	DY4	4/18/2013	-139.45	59.09	Surface	0.97			
DY	DY4	4/19/2013	-139.49	59.16	Surface	2.84			
DY	DY4	4/19/2013	-139.55	59.26	Surface	1.99			
DY	DY4	4/19/2013	-139.62	59.36	Surface	1.11			
DY	DY5	4/22/2013	-141.44	59.70	Surface	1.79			
DY	DY5	4/22/2013	-141.58	59.69	Surface	1.5			
DY	DY5	4/22/2013	-141.73	59.68	Surface	1.19			
DY	DY5	4/22/2013	-141.89	59.67	Surface	0.9			
DY	DY5	4/22/2013	-142.06	59.66	Surface	0.6			
DY	DY5	4/22/2013	-142.22	59.65	Surface	0.65			
DY	DY5	4/22/2013	-142.38	59.64	Surface	0.52			
DY	DY5	4/22/2013	-142.54	59.63	Surface	0.58			
DY	DY5	4/22/2013	-142.73	59.62	Surface	0.66			
DY	DY5	4/22/2013	-142.88	59.61	Surface	0.54			
DY	DY5	4/22/2013	-143.05	59.60	Surface	0.47			
DY	DY5	4/23/2013	-143.19	59.59	Surface	0.38			
DY	DY5	4/23/2013	-143.35	59.58	Surface	0.54			
DY	DY5	4/23/2013	-143.52	59.57	Surface	0.64			
DY	DY5	4/23/2013	-143.73	59.56	Surface	0.63			

APPENDIX B: Surface transects iron data for Cruise 1TX during the late spring 2013.

Cruise	Transect	Date	Longitude [degrees_east]	Latitude [degrees_north]	Depth [m]	DFe [nM]	LPFe[nM]	RPFe[nM]	TPFe[nM]
1TX	1TX1	4/26/2013	-150.14	58.90	Surface	0.772			
1TX	1TX1	4/26/2013	-150.25	58.70	Surface	0.586			
1TX	1TX1	4/26/2013	-150.30	58.61	Surface	1.304			
1TX	1TX1	4/26/2013	-150.41	58.47	Surface	1.077			
1TX	1TX2	4/27/2013	-150.79	57.68	Surface	1.039			
1TX	1TX2	4/27/2013	-150.88	57.55	Surface	1.096			
1TX	1TX2	4/27/2013	-151.00	57.39	Surface	1.047			
1TX	1TX2	4/27/2013	-151.11	57.25	Surface	1.333			
1TX	1TX2	4/27/2013	-151.21	57.11	Surface	0.51			
1TX	1TX2	4/27/2013	-151.29	56.96	Surface	0.872			
1TX	1TX2	4/27/2013	-151.37	56.80	Surface	0.444			
1TX	1TX3	4/30/2013	-151.93	57.63	Surface	1.71			
1TX	1TX3	4/30/2013	-151.79	57.62	Surface	0.81			
1TX	1TX3	4/30/2013	-151.65	57.60	Surface	1.01			
1TX	1TX3	4/30/2013	-151.51	57.59	Surface	0.88			
1TX	1TX3	4/30/2013	-151.34	57.57	Surface	1.32			
1TX	1TX4	5/3/2013	-150.13	59.36	Surface	1.6			
1TX	1TX4	5/3/2013	-150.03	59.31	Surface	1.07			
1TX	1TX4	5/3/2013	-149.94	59.27	Surface	0.94			
1TX	1TX4	5/3/2013	-149.83	59.22	Surface	1.05			
1TX	1TX4	5/3/2013	-149.72	59.12	Surface	1.66			
1TX	1TX4	5/3/2013	-149.62	59.08	Surface	1.05			
1TX	1TX4	5/3/2013	-149.52	59.03	Surface	0.76			
1TX	1TX4	5/3/2013	-149.43	58.96	Surface	2.72			
1TX	1TX4	5/3/2013	-149.32	58.91	Surface	2.74			
1TX	1TX4	5/3/2013	-149.22	58.86	Surface	2.78			
1TX	1TX4	5/3/2013	-149.12	58.82	Surface	0.45			
1TX	1TX5	5/4/2013	-147.81	58.14	Surface	1.18			
1TX	1TX5	5/4/2013	-147.89	58.20	Surface	0.31			
1TX	1TX5	5/4/2013	-147.92	58.23	Surface	0.42			
1TX	1TX5	5/4/2013	-148.02	58.32	Surface	0.3			
1TX	1TX5	5/4/2013	-148.06	58.38	Surface	0.29			
1TX	1TX5	5/4/2013	-148.12	58.45	Surface	0.77			
1TX	1TX5	5/4/2013	-148.17	58.51	Surface	0.52			
1TX	1TX5	5/4/2013	-148.24	58.56	Surface	0.35			
1TX	1TX5	5/4/2013	-148.32	58.65	Surface	0.62			
1TX	1TX5	5/5/2013	-148.75	59.11	Surface	1.14			
1TX	1TX5	5/5/2013	-148.70	59.06	Surface	0.61			
1TX	1TX5	5/5/2013	-148.64	59.01	Surface	1.03			
1TX	1TX5	5/5/2013	-148.61	58.98	Surface	1			
1TX	1TX5	5/6/2013	-149.41	59.78	Surface	2.17			
1TX	1TX5	5/6/2013	-149.34	59.71	Surface	0.89			
1TX	1TX5	5/6/2013	-149.25	59.61	Surface	0.59			

APPENDIX B: continued

Cruise	Transect	Date	Longitude [degrees_east]	Latitude [degrees_north]	Depth [m]	DFe [nM]	LPFe[nM]	RPFe[nM]	TPFe[nM]
1TX	1TX5	5/6/2013	-149.20	59.57	Surface	0.95	11.73	84.9	96.63
1TX	1TX5	5/6/2013	-149.13	59.49	Surface	0.34			
1TX	1TX5	5/6/2013	-149.07	59.43	Surface	0.6	3.7	48.35	52.05
1TX	1TX5	5/6/2013	-149.00	59.33	Surface	0.39			
1TX	1TX5	5/6/2013	-148.94	59.26	Surface	0.4	1.79	22.34	24.13
1TX	1TX5	5/6/2013	-148.84	59.18	Surface	0.65			
1TX	1TX5	5/6/2013	-148.78	59.13	Surface	0.78	6.53	74.45	80.98
1TX	1TX5	5/6/2013	-148.70	59.05	Surface	1.62			
1TX	1TX5	5/6/2013	-148.64	58.99	Surface	2.01	22.65	65.26	87.9
1TX	1TX5	5/6/2013	-148.57	58.89	Surface	1.1			
1TX	1TX5	5/6/2013	-148.51	58.82	Surface	1.82	6.5	75.15	81.65
1TX	1TX6	5/6/2013	-148.46	58.86	Surface	1.39			
1TX	1TX6	5/6/2013	-148.43	58.93	Surface	1.49			
1TX	1TX6	5/6/2013	-148.40	59.00	Surface	1.17			
1TX	1TX6	5/6/2013	-148.36	59.08	Surface	0.96			
1TX	1TX6	5/6/2013	-148.33	59.15	Surface	1.06			
1TX	1TX6	5/6/2013	-148.29	59.23	Surface	1.3			
1TX	1TX6	5/6/2013	-148.25	59.30	Surface	1.2			
1TX	1TX6	5/6/2013	-148.21	59.37	Surface	1.96			
1TX	1TX6	5/6/2013	-148.18	59.45	Surface	1.5			
1TX	1TX6	5/6/2013	-148.14	59.53	Surface	1.37			
1TX	1TX6	5/6/2013	-148.11	59.62	Surface	1.23			
1TX	1TX6	5/6/2013	-148.06	59.69	Surface	1.75			
1TX	1TX6	5/6/2013	-148.01	59.76	Surface	1.31			
1TX	1TX6	5/6/2013	-147.96	59.83	Surface	2.3			
1TX	1TX6	5/6/2013	-147.92	59.86	Surface	2.86			

APPENDIX C: Iron data from the vertical depth profiles collected during Cruise DY in the late spring 2013.

Cruise	Station Name	Date	Longitude [degrees_east]	Latitude [degrees_north]	Depth [m]	DFe [nM]	LPFe [nM]	RPFe [nM]	TPFe [nM]
DY	sek20	4/8/2013	-137.19	57.80	15	0.84	2.79	14.07	16.86
DY	sek20	4/8/2013	-137.19	57.80	30	1.49	3.65	12.41	16.06
DY	sek20	4/8/2013	-137.19	57.80	50	1.02	3.11	7.84	10.96
DY	sek5	4/8/2013	-136.79	57.92	15	1.33	2.22	9.36	11.58
DY	sek5	4/8/2013	-136.79	57.92	30	1.25	2.68	10.59	13.27
DY	sek5	4/8/2013	-136.79	57.92	50	0.70	0.72	3.79	4.51
DY	seg20	4/11/2013	-136.60	57.20	20	0.98	5.22	15.77	20.99
DY	seg20	4/11/2013	-136.60	57.20	45	1.24	5.87	19.00	24.87
DY	seg10	4/11/2013	-136.35	57.28	100	0.66	2.10	8.87	10.97
DY	seg5.0	4/11/2013	-136.20	57.32	20	1.34	5.88	9.64	15.52
DY	seg5.0	4/11/2013	-136.20	57.32	45	2.15	6.99	27.91	34.90
DY	seg5.0	4/11/2013	-136.20	57.32	75	1.58	4.67	17.55	22.22
DY	seg5.0	4/11/2013	-136.20	57.32	100	1.47	4.58	14.91	19.49
DY	seg5.0	4/11/2013	-136.20	57.32	150	7.19	6.06	19.91	25.98
DY	sea20	4/14/2013	-135.71	56.32	15	1.78	7.82	25.17	32.98
DY	sea20	4/14/2013	-135.71	56.32	30	2.42	7.56	21.57	29.13
DY	sea20	4/14/2013	-135.71	56.32	50	2.39	6.25	29.45	35.70
DY	sea20	4/14/2013	-135.71	56.32	100	1.94	6.56	24.82	31.38
DY	sea20	4/14/2013	-135.71	56.32	150	2.32	7.39	30.92	38.32
DY	sea20	4/14/2013	-135.71	56.32	350	1.66	6.96	29.55	36.51
DY	sea20	4/14/2013	-135.71	56.32	500	1.30	5.62	20.85	26.47
DY	sea5	4/14/2013	-135.33	56.44	15	2.36	4.05	11.71	15.77
DY	sea5	4/14/2013	-135.33	56.44	30	2.21	3.88	9.96	13.85
DY	sea5	4/14/2013	-135.33	56.44	50	1.89	5.21	7.03	12.24
DY	sea5	4/14/2013	-135.33	56.44	75	3.93	6.84	18.30	25.13
DY	sea5	4/14/2013	-135.33	56.44	100	2.24	10.38	35.84	46.22
DY	sea40	4/16/2013	-136.22	56.14	20	0.53	0.47	2.82	3.30
DY	sea40	4/16/2013	-136.22	56.14	50	0.22	0.12	0.64	0.75
DY	sea40	4/16/2013	-136.22	56.14	75	0.44	0.49	0.89	1.37
DY	sea40	4/16/2013	-136.22	56.14	100	0.36	0.26	0.72	0.99
DY	sea40	4/16/2013	-136.22	56.14	200	0.46	0.20	0.62	0.82
DY	sea40	4/16/2013	-136.22	56.14	300	0.58	0.80	3.90	4.70
DY	sea40	4/16/2013	-136.22	56.14	500	0.69	0.36	1.92	2.28
DY	seg20	4/16/2013	-136.57	57.20	20	0.88	1.93	6.90	8.83
DY	seg20	4/16/2013	-136.57	57.20	45	0.49	1.45	6.53	7.99
DY	seg20	4/16/2013	-136.57	57.20	100	0.50	2.72	7.46	10.19
DY	seg20	4/16/2013	-136.57	57.20	200	0.78	2.27	12.56	14.84
DY	seg20	4/16/2013	-136.57	57.20	300	0.66	1.58	7.18	8.76
DY	sek30	4/17/2013	-137.50	57.71	15	1.21	3.04	12.84	15.88
DY	sek30	4/17/2013	-137.50	57.71	30	1.04	2.84	13.43	16.27
DY	sek30	4/17/2013	-137.50	57.71	100	0.97	3.96	12.82	16.78
DY	sek30	4/17/2013	-137.50	57.71	150	1.15	5.38	15.21	20.59
DY	sek30	4/17/2013	-137.50	57.71	300	1.75	13.26	43.22	56.48
DY	sek30	4/17/2013	-137.50	57.71	500	0.79	2.52	20.75	23.27
DY	ybc50	4/19/2013	-140.79	58.80	20	2.55	0.88	8.48	9.36
DY	ybc50	4/19/2013	-140.79	58.80	40	1.87	1.85	9.54	11.39
DY	ybc50	4/19/2013	-140.79	58.80	70	0.91	2.66	19.17	21.83
DY	ybc50	4/19/2013	-140.79	58.80	100	1.54	4.71	31.40	36.11
DY	ybc50	4/19/2013	-140.79	58.80	130	0.91	3.45	23.28	26.73
DY	ybc50	4/19/2013	-140.79	58.80	170	1.29	4.18	14.35	18.53
DY	ybc30	4/19/2013	-140.44	59.06	15	0.59	1.46	11.91	13.37
DY	ybc30	4/19/2013	-140.44	59.06	30	1.28	1.16	9.87	11.03
DY	ybc30	4/19/2013	-140.44	59.06	50	1.02	2.87	16.65	19.52
DY	ybc30	4/19/2013	-140.44	59.06	75	0.94	1.54	10.67	12.20
DY	ybc30	4/19/2013	-140.44	59.06	110	6.75	4.10	37.51	41.61

APPENDIX C. continued

Cruise	Station Name	Date	Longitude [degrees_east]	Latitude [degrees_north]	Depth [m]	DFe [nM]	LPFe [nM]	RPFe [nM]	TPFe [nM]
DY	ybc10	4/20/2013	-140.07	59.35	15	1.51	1.56	13.05	14.60
DY	ybc10	4/20/2013	-140.07	59.35	100	1.62	11.90	81.14	93.04
DY	ybc10	4/20/2013	-140.07	59.35	130	1.34	4.34	40.13	44.47
DY	ybe40	4/21/2013	-141.19	59.11	30	0.89	0.20	2.13	2.33
DY	ybe40	4/21/2013	-141.19	59.11	65	0.18	0.63	1.99	2.61
DY	ybe40	4/21/2013	-141.19	59.11	100	1.54	5.46	19.58	25.04
DY	kia4	4/23/2013	-143.92	59.55	15	0.43	0.40	3.12	3.52
DY	kia4	4/23/2013	-143.92	59.55	30	0.21	0.40	3.36	3.76
DY	kia4	4/23/2013	-143.92	59.55	50	0.29	0.25	4.46	4.71
DY	kia4	4/23/2013	-143.92	59.55	100	0.14	0.25	2.25	2.49
DY	kia4	4/23/2013	-143.92	59.55	150	0.38	1.82	11.27	13.09
DY	kia4	4/23/2013	-143.92	59.55	300	0.48	7.39	40.04	47.43
DY	kiba	4/23/2013	-144.91	59.87	15	26.53	42.22	451.62	493.84
DY	kiba	4/23/2013	-144.91	59.87	30	44.27	53.13	379.95	433.08
DY	kiba	4/23/2013	-144.91	59.87	65	33.13	106.89	632.47	739.35
DY	kiba	4/23/2013	-144.91	59.87	110	32.72	77.60	783.55	861.15

APPENDIX D: Iron data from the vertical depth profiles collected during Cruise 1TX in the late spring 2013

Cruise	Station Name	Date	Longitude [degrees_east]	Latitude [degrees_north]	Depth [m]	DFe [nM]	LPFe [nM]	RPFe [nM]	TPFe [nM]
1TX	181-HL	4/27/2013	-152.89	57.05	15	0.69	4.19	21.07	25.25
1TX	181-HL	4/27/2013	-152.89	57.05	30	0.77	8.80	14.81	23.61
1TX	181-HL	4/27/2013	-152.89	57.05	45	1.74	16.77	187.13	203.91
1TX	181-HL	4/27/2013	-152.89	57.05	60	2.05	20.54	201.58	222.12
1TX	185-HX	4/27/2013	-151.19	56.60	15	0.54	0.33	7.09	7.42
1TX	185-HX	4/27/2013	-151.19	56.60	30	0.46	0.67	11.85	12.52
1TX	185-HX	4/27/2013	-151.19	56.60	50	0.22	0.52	3.91	4.43
1TX	197-HT	4/30/2013	-150.34	57.55	20	0.79	15.80	178.96	194.76
1TX	197-HT	4/30/2013	-150.34	57.55	40	0.81	16.01	225.69	241.70
1TX	197-HT	4/30/2013	-150.34	57.55	75	0.98	18.11	204.75	222.86
1TX	197-HT	4/30/2013	-150.34	57.55	150	1.10	43.78	149.22	193.00
1TX	197-HL	4/30/2013	-151.18	58.01	20	0.74	44.30	267.63	311.93
1TX	197-HL	4/30/2013	-151.18	58.01	40	0.56	36.50	282.34	318.84
1TX	197-HL	4/30/2013	-151.18	58.01	50	0.77	21.18	331.18	352.36
1TX	GAK 13	5/3/2013	-147.78	58.10	80	1.25	1.17	10.32	11.49
1TX	GAK 13	5/3/2013	-147.78	58.10	110	0.67	1.25	8.60	9.85
1TX	GAK 13	5/3/2013	-147.78	58.10	150	0.78	0.44	2.85	3.29
1TX	GAK 1	5/5/2013	-149.47	59.84	25	1.00	6.62	62.72	69.34
1TX	GAK 1	5/5/2013	-149.47	59.84	50	1.31	5.00	89.16	94.16
1TX	GAK 1	5/5/2013	-149.47	59.84	100	1.82	7.84	84.07	91.90
1TX	GAK 1	5/5/2013	-149.47	59.84	190	2.81	7.84	219.24	227.07
1TX	CG	5/7/2013	-147.07	60.98	1	1.84	161.05	921.96	1083.02
1TX	CG	5/7/2013	-147.07	60.98	20	7.61	279.74	464.72	744.46
1TX	CG	5/7/2013	-147.07	60.98	55	5.35	54.13	315.64	369.77
1TX	CG	5/7/2013	-147.07	60.98	95	1.96	37.80	414.21	452.01
1TX	CG	5/7/2013	-147.07	60.98	155	3.21	48.81	311.90	360.70

APPENDIX E: Surface transects iron data for Cruise 2TX in the early fall 2013.

Cruise	Transect	Date	Longitude [degrees_east]	Latitude [degrees_north]	Depth [m]	DFe [nM]	LPFe [nM]	RPFe [nM]	TPFe [nM]
2TX	2TX1	9/16/2013	-136.8467	57.12466	Surface	0.29			
2TX	2TX1	9/16/2013	-136.60491	57.19719	Surface	0.5			
2TX	2TX1	9/16/2013	-136.357	57.27749	Surface	0.07			
2TX	2TX1	9/16/2013	-136.21803	57.31974	Surface	0.84			
2TX	2TX1	9/16/2013	-136.0816	57.35977	Surface	0.65			
2TX	2TX2	9/16/2013	-136.54724	56.84189	Surface	0.39			
2TX	2TX2	9/17/2013	-136.31303	56.90266	Surface	0.18			
2TX	2TX2	9/17/2013	-136.05263	56.99078	Surface	0.31			
2TX	2TX2	9/17/2013	-135.97866	57.00154	Surface	0.76			
2TX	2TX3	9/17/2013	-135.55091	56.75098	Surface	0.23			
2TX	2TX3	9/17/2013	-135.6116	56.73418	Surface	0.62			
2TX	2TX3	9/17/2013	-135.79303	56.68036	Surface	0.12			
2TX	2TX3	9/17/2013	-136.01002	56.61022	Surface	0.6			
2TX	2TX3	9/17/2013	-136.23494	56.52531	Surface	0.57			
2TX	2TX4	9/18/2013	-135.89401	56.24123	Surface	0.47			
2TX	2TX4	9/18/2013	-135.67138	56.32153	Surface	0.2			
2TX	2TX4	9/18/2013	-135.4448	56.40011	Surface	0.3			
2TX	2TX4	9/18/2013	-135.27678	56.44604	Surface	0.52			
2TX	2TX4	9/18/2013	-135.20876	56.47706	Surface	0.61			
2TX	2TX5	9/18/2013	-137.04404	57.43761	Surface	0.63			
2TX	2TX5	9/18/2013	-137.56328	57.67628	Surface	0.18			
2TX	2TX5	9/18/2013	-137.96658	57.88694	Surface	0.29			
2TX	2TX5	9/19/2013	-138.4498	58.07129	Surface	0.15			
2TX	2TX5	9/19/2013	-139.00575	58.23689	Surface	0.14			
2TX	2TX5	9/19/2013	-139.56108	58.40608	Surface	0.3			
2TX	2TX5	9/19/2013	-140.11436	58.59436	Surface	0.35			
2TX	2TX6	9/19/2013	-140.7988	58.80631	Surface	0.86			
2TX	2TX6	9/19/2013	-140.60568	58.92403	Surface	0.29			
2TX	2TX6	9/19/2013	-140.44531	59.08611	Surface	0.41			
2TX	2TX6	9/19/2013	-140.25161	59.21893	Surface	0.24			
2TX	2TX6	9/19/2013	-139.90876	59.48311	Surface	2.96			
2TX	2TX6	9/20/2013	-140.09636	59.3565	Surface	0.63			
2TX	2TX7	9/20/2013	-141.15613	59.34608	Surface	0.4			
2TX	2TX7	9/20/2013	-142.11558	59.3545	Surface	0.34			
2TX	2TX7	9/20/2013	-142.99	59.35308	Surface	0.26			
2TX	2TX7	9/20/2013	-143.94896	59.35706	Surface	0.13			
2TX	2TX8	9/20/2013	-144.89905	59.34966	Surface	0.26			
2TX	2TX8	9/20/2013	-144.94327	59.47823	Surface	0.28			
2TX	2TX8	9/20/2013	-144.92713	59.60858	Surface	3.29			
2TX	2TX8	9/20/2013	-144.90956	59.73234	Surface	2.3			
2TX	2TX9	9/21/2013	-145.3672	59.94814	Surface	2.67			
2TX	2TX9	9/21/2013	-145.612	60.02779	Surface	3.75			
2TX	2TX9	9/21/2013	-145.90311	60.08486	Surface	3.32			
2TX	2TX9	9/21/2013	-146.19033	60.13993	Surface	2.72			
2TX	2TX9	9/21/2013	-146.44729	60.18284	Surface	4.05			
2TX	2TX9	9/21/2013	-146.70419	60.24429	Surface	3.8			

APPENDIX E: continued

Cruise	Transect	Date	Longitude [degrees_east]	Latitude [degrees_north]	Depth [m]	DFe [nM]	LPFe [nM]	RPFe [nM]	TPFe [nM]
2TX	2TX9	9/21/2013	-147.06368	60.96	Surface		479.2	4301.49	4780.69
2TX	2TX10	9/24/2013	-147.81486	58.08238	Surface		3	131.25	134.25
2TX	2TX10	9/24/2013	-147.92763	58.23193	Surface				
2TX	2TX10	9/24/2013	-148.08049	58.37714	Surface		0.18	38.18	38.36
2TX	2TX10	9/24/2013	-148.16875	58.49924	Surface				
2TX	2TX10	9/24/2013	-148.38726	58.68003	Surface		0.98	44.99	45.97
2TX	2TX10	9/24/2013	-148.49024	58.80484	Surface				
2TX	2TX10	9/24/2013	-148.61464	58.97144	Surface		0.56	21.1	21.66
2TX	2TX10	9/24/2013	-148.73733	59.08451	Surface				
2TX	2TX10	9/26/2013	-148.94106	59.24729	Surface		2.49	25.37	27.86
2TX	2TX10	9/26/2013	-149.05321	59.40269	Surface				
2TX	2TX10	9/26/2013	-149.17176	59.53648	Surface	0.86	1.27	50.82	52.09
2TX	2TX10	9/26/2013	-149.35333	59.69041	Surface	5.44			
2TX	2TX10	9/26/2013	-149.47443	59.84513	Surface	5.86	8.73	210.08	218.81

Chapter 3: Conclusion

The partitioning of Fe size classes over the GOA shelf was distinct within each surveyed region, with increasing average concentrations of PFe moving from the Southeastern to the Western region (Figure 3.1). This trend follows the abundance of glaciated watersheds and the path of the ACC, which transports particulate rich waters. Within PWS, samples were dominated by glacial discharge that introduces significant amounts of Fe rich glacial particulates into surface waters. Likewise, areas with enhanced glacial input over the Northern and Western shelves displayed increasingly elevated Fe signals across the size classes. The variability observed in the DFe class is likely due to a combination of local geographic features that influence oceanographic processes, as well as the biological activity. In the absence of high glacial influence like over the Southeastern shelf, TPFe was considerably less abundant. The similarity in the LPFe fraction over the Northern and Western shelves further indicates glacial influence, as has previously been observed to be ~ 11 % of the TPFe (Lippiatt et al., 2010). However, in

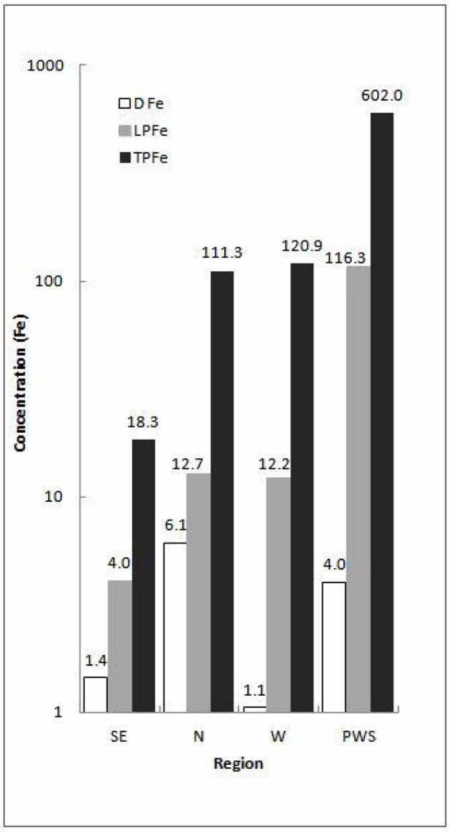

Figure 3.1: Average Fe concentrations for the different size classes present along the Southeastern (SE), Northern (N), and Western (W) shelves, and Prince William Sound (PWS).

the early fall, results indicate the contribution of LPFe to the reactive Fe pool was not as high as has been previously observed in the late summer (Lippiatt et al., 2010). This can be a result of our sampling not taking place in low salinity river plumes. Future work should consider identifying and understanding what processes are affecting the LPFe distribution over the Northern and Western shelves later in the season.

The shelf and slope system in the Southeast, with a poorly defined ACC and complex bathymetry, creates a dynamic system providing a stage for multiple oceanographic processes that impact the distribution of Fe. Here the spatial distribution of Fe at the surface and at depth were observed to be related to the location of the ACC, downwelling, bathymetric influenced intense mixing near Cross Sound, circulation patterns near Chatham Strait, and periods of downwelling relaxation. Because of the narrow shelf and downwelling, signals from re-suspended shelf sediments are observable along the slope and offshore indicating transport of these Fe rich sediments into the interior basin of the GOA. The predominance of downwelling contributes to the buffering of shelf water which transports reactive Fe along the shelf and slope system. During the episodic periods of downwelling relaxation, Fe rich surface waters can move into the central GOA possibly having implications with offshore production. A future focus on the effect of downwelling/upwelling events and how these affect the transport of DFe over the Southeastern shelf and slope system is recommended. Additionally, these occurrences likely have an impact on offshore surface waters. Future studies should be conducted to understand to what extent the subsurface transport of re-suspended shelf sediments can influence interior GOA basin waters.

Over a portion of the wider and shallower Northern shelf, near Yakutat Bay in the late spring, cross shelf flows are a likely contributor to the transport of subsurface re-suspended sediments which increased the TPFe signal ~ 100 m depth at all of the stations across the shelf. Further northwest on either side of Kayak Island, very different Fe distributions are observed. This is due in part to the placement of the stations sampled. Very high TPFe and LPFe were found on the northwest side of Kayak Island where it is directly influenced by the Copper River discharge which transports sediment laden waters several hundred meters over the shelf. On the southeast side of Kayak Island, substantially less TPFe and LPFe were found over the slope, which likely has influences from offshore waters. However, the distinct PFe signal at depth indicates that shelf sediment re-suspension occurs here. During the early fall, elevated DFe and low salinity along the transects leaving the mouth of PWS and in the vicinity of the Copper River means surface waters are recharged by freshwater input. There was a distinct drop in DFe concentration as Transect 2TX8 neared the slope. Future work along this part of the Northern shelf should include investigating particulate Fe distributions at depth.

The presence of troughs and canyons along the Western shelf and the diminished influence of the ACC along the southern side of Kodiak Island creates complex flows along the wide portion of the shelf perpendicular to Kodiak Island that contributes to the observed distributions of Fe here. Cross shelf

transport of Fe species is visible along much of the shelf but immediate reductions in concentrations over the slope. The higher salinities over the slope indicate influences from offshore circulation. Since vertical profiles were not taken at deeper depths over the slope, future studies should discover what oceanographic processes control Fe partitioning at depth. Overall, this study provides a clearer picture of the highly seasonal input and geographic disparity of Fe distributions.

References

Aciego, S. M., E. I. Stevenson, and C. A. Arendt. 2015. Climate versus geological controls on glacial meltwater micronutrient production in southern Greenland. Earth Planet. Sci. Lett. **424**: 51–58. doi:10.1016/j.epsl.2015.05.017

Aguilar-Islas, A. M., M. J. M. Seguret, R. Rember, K. N. Buck, P. Proctor, C. W. Mordy, and N. B. Kachel. 2016. Temporal variability of reactive iron over the Gulf of Alaska shelf. Deep. Res. Part II Top. Stud. Oceanogr. 132: 90–106.

Armbrust, E. V., J. A. Berges, C. Bowler, and others. 2004. The Genome of the Diatom Thalassiosira Pseudonona: Ecology, Evolution, and Metabolsim. Science **306**: 79–85.

Barbeau, K. 2006. Photochemistry of organic iron(III) complexing ligands in oceanic systems. Photochem. Photobiol. **82**: 1505–1516. doi:10.1562/2006-06-16-IR-935

Berger, C. J. M., S. M. Lippiatt, M. G. Lawrence, and K. W. Bruland. 2008. Application of a chemical leach technique for estimating labile particulate aluminum, iron, and manganese in the Columbia River plume and coastal waters off Oregon and Washington. J. Geophys. Res. **113**: C00B01. doi:10.1029/2007JC004703

Boyle, E. A., J. M. Edmond, and E. R. Sholkovitz. 1977. The mechanism of iron removal in estuaries. Geochim. Cosmochim. Acta **41**: 1313–1324. doi:10.1016/0016-7037(77)90075-8

Boyd, P. W., A. J. Watson, C. S. Law, and others. 2000. A mesoscale phytoplankton bloom in the polar Southern Ocean stimulated by iron fertilization. Nature **407**: 695–702. doi:10.1038/35037500

Boyd, P. W., C. S. Law, C. S. Wong, and others. 2004. The decline and fate of an iron-induced subarctic phytoplankton bloom. Nature **428**: 549–553. doi:10.1029/2001JB001129

Boyd, P. W., T. Jickells, C. S. Law, and others. 2007. REVIEW Mesoscale Iron Enrichment Experiments 1993 – 2005: Synthesis and Future Directions. **315**: 612–618.

Brown, M. T., S. M. Lippiatt, M. C. Lohan, and K. W. Bruland. 2012. Trace metal distributions within a Sitka eddy in the northern Gulf of Alaska. Limnol. Ocean. **57**: 503–518. doi:10.4319/lo.2012.57.2.0503

Bruland K. W. and Rue E. L. 2001. Iron: analytical methods for the determination of concentrations and speciation. In The Biogeochemistry of Iron in Seawater (eds. K. A. Hunter and D. R. Turner). John Wiley and Sons, 255, p. 289.

Buck, K.N., Lohan, M.C., Berger, C.J.M., and Bruland, K.W. 2007. Dissolved iron speciation in two distinct river plumes and an estuary: implications for riverine iron supply. Limnol. Oceanogr. 52, 843–855.

Brzezinski, M. A., C. J. Pride, and V. M. Franck. 2002. A switch from Si(OH)4 to NO3- depletion in the glacial Southern Ocean. Geophys. Res. Lett. **29**: 3–6. doi:0094-8276/02/2001GL014349

Clarke, F. W., and H. S. Washington. 1924. The composition of the Earth's crust. United States Geol. Surv.

Christensen, H.H., Mastrantonio, L., Gordon, J.C., and Bormann, B.T. 2000. Alaska's Copper River: Humankind in a Changing World. United States Department of Agriculture. General Technical Report, PNW-GTR-480, 20 pp.

Coale, K. H., K. S. Johnson, S. E. Fitzwater, and others. 1996. A massive phytoplankton bloom induced by an ecosystem scale iron fertilization experiment in the equatorial Pacific Ocean. Nature **383**: 495–501. doi:10.1038/383495a0

Crusius, J., A. W. Schroth, S. Gassó, C. M. Moy, R. C. Levy, and M. Gatica. 2011. Glacial flour dust storms in the Gulf of Alaska : Hydrologic and meteorological controls and their importance as a source of bioavailable iron. Geophys. Res. Lett. **38**: 1–5. doi:10.1029/2010GL046573

de Baar, H. J. W., P. W. Boyd, K. H. Coale, and others. 2005. Synthesis of iron fertilization experiments: From the iron age in the age of enlightenment. J. Geophys. Res. C Ocean. **110**: 1–24. doi:10.1029/2004JC002601

Elrod, V. A., W. M. Berelson, K. H. Coale, and K. S. Johnson. 2004. The flux of iron from continental shelf sediments: A missing source for global budgets. Geophys. Res. Lett. **31**: 2–5. doi:10.1029/2004GL020216

Field, C. B., M. J. Behrenfeld, J. T. Randerson, P. Falkowski, C. B. Field, M. J. Behrenfeld, and J. T. Randerson. 2011. Primary Production of the Biosphere : Integrating Terrestrial and Oceanic Components. **281**: 237–240.

Hill, D. F., N. Bruhis, C. S.E., a. a. Arendt, and J. Beamer. 2015. Spatial and temporal variability of freshwater discharge into the Gulf of Alaska. J. Geophys. Res. Ocean. 634–646. doi:10.1002/2014JC010395

Hood, E., and D. Scott. 2008. Riverine organic matter and nutrients in southeast Alaska affected by glacial coverage. Nat. Geosci. **1**: 583–587. doi:10.1038/ngeo280

Hurst, M.P. and K.W. Bruland. 2007. An investigation into the exchange of iron and zinc between soluble, colloidal, and particulate size-fractions in shelf waters using low-abundance isotopes as tracers in shipboard incubation experiments. Mar. Chem. 103: 211-226.

Hurst, M. P., A. M. Aguilar-Islas, and K. W. Bruland. 2010. Iron in the southeastern Bering Sea: Elevated leachable particulate Fe in shelf bottom waters as an important source for surface waters. Cont. Shelf Res. **30**: 467–480. doi:10.1016/j.csr.2010.01.001

Johnson, K. S., R. Michael Gordon, and K. H. Coale. 1997. What controls dissolved iron concentrations in the world ocean? Mar. Chem. **57**: 137–161. doi:10.1016/S0304-4203(97)00043-1

Johnson, K. W., N. E. Sutherland, C.S. Wong, L. A. M. 2005. Iron transport by mesoscale Haida eddies in the Gulf of Alaska. Deep. Res. Part II **52**: 933–953. doi:10.1016/j.dsr2.2004.08.017

Ladd, C., P. Stabeno, and E. D. Cokelet. 2005. A note on cross-shelf exchange in the northern Gulf of Alaska. Deep. Res. II. **52**: 667–679. doi:10.1016/j.dsr2.2004.12.022

Ladd, C., W. R. Crawford, C. E. Harpold, W. K. Johnson, N. B. Kachel, P. J. Stabeno, and F. Whitney. 2009. A synoptic survey of young mesoscale eddies in the Eastern Gulf of Alaska. Deep Sea Res. Part II Top. Stud. Oceanogr. **56**: 2460–2473. doi:10.1016/j.dsr2.2009.02.007

Lagerström, M. E., M. P. Field, M. Séguret, L. Fischer, S. Hann, and R. M. Sherrell. 2013. Automated on-line fl ow-injection ICP-MS determination of trace metals (Mn, Fe, Co, Ni, Cu and Zn) in open ocean seawater : Application to the GEOTRACES program. Mar. Chem. **155**: 71–80. doi:10.1016/j.marchem.2013.06.001

Lam, P. J., J. K. B. Bishop, C. C. Henning, M. A. Marcus, G. A.Waychunas, and I. Y. Fung. 2006. Wintertime phytoplankton bloom in the subarctic Pacific supported by continental margin iron, Global Biogeochem. Cycles, 20, GB1006, doi:10.1029/2005GB002557.

Landry, M. R., R. T. Barber, R. Bidigare, and others. 1997. Iron and grazing constraints on primary production in the central equatorial Pacific: An EqPac synthesis. Limnol. Oceanogr. **42**: 405–418. doi:10.4319/lo.1997.42.3.0405

Lippiatt, S. M., M. C. Lohan, and K. W. Bruland. 2010. The distribution of reactive iron in northern Gulf of Alaska coastal waters. Mar. Chem. **121**: 187–199. doi:10.1016/j.marchem.2010.04.007

Lippiatt, S. M., M. T. Brown, M. C. Lohan, and K. W. Bruland. 2011. Reactive iron delivery to the Gulf of Alaska via a Kenai eddy. Deep. Res. Part I **58**: 1091–1102. doi:10.1016/j.dsr.2011.08.005

Martin, J. H., R. M. Gordon, S. Fitzwater, and W. W. Broenkow. 1989. Vertex: phytoplankton/iron studies in the Gulf of Alaska. Deep Sea Res. Part A. Oceanogr. Res. Pap. **36**: 649–680. doi:10.1016/0198-0149(89)90144-1

Martin, J. H. 1990. GLACIAL- INTERGLACIAL CO_2 CHANGE: the Iron Hypothesis. Paleoceanography **5**: 1–13.

Martin, J. H., K. H. Coale, K. S. Johnson, and others. 1994. Testing the iron hypothesis in ecosystems of the equatorial Pacific Ocean. Nature **371**: 123–129.

Millero, F. J., W. Yao, and J. Aicher. 1995. The speciation of Fe(II) and Fe(III) in natural waters. Mar. Chem. **50**: 21–39. doi:10.1016/0304-4203(95)00024-L

Millero, F. J. 1998. Solubility of Fe(III) in seawater. Earth Planet. Sci. Lett. **154**: 323–329. doi:10.1016/S0012-821X(97)00179-9

Milne, A., C. Schlosser, B. D. Wake, E. P. Achterberg, R. Chance, A. R. Baker, A. Forryan, and M. C. Lohan. 2017. Particulate phases are key in controlling dissolved iron concentrations in the (sub)tropical North Atlantic. Geophys. Res. Lett. 44: 2377–2387.

Moore, J. K., S. C. Doney, D. M. Glover, and I. Y. Fung. 2002. Iron cycling and nutrient-limitation patterns in surface waters of the world ocean. Deep. Res. Part II Top. Stud. Oceanogr. **49**: 463–507. doi:10.1016/S0967-0645(01)00109-6

Mote, P. W., E. A. Parson, A. F. Hamlet, and others. 2003. Forests of the Pacific Northwest. Clim. Change **61**: 45–88.

Morel, F. M. M., J. G. Rueter, and N. M. Price. 1991. Iron nutrition of phytoplankton and its possible importance in the ecology of ocean regions with high nutrient and low biomass. Oceanography **4**: 56–61. doi:10.5670/oceanog.1991.03

Naidu, A. S., and T. C. Mowatt. 1983. Sources and dispersal patterns of clay minerals in surface sediments from the continental-shelf areas off Alaska. Geol. Soc. Am. Bull. **94**: 841–854. doi:10.1130/0016-7606(1983)94<841:SADPOC>2.0.CO;2

Neal, E. G., E. Hood, and K. Smikrud. 2010. Contribution of glacier runoff to freshwater discharge into the Gulf of Alaska. Geophys. Res. Lett. **37**: 1–5. doi:10.1029/2010GL042385

Nelson, D. M., P. Treguer, M. A. Brzezinski, A. Leynaert, and B. Queguiner. 1995. Production and dissolution of biogenic silica in the ocean: Revised global estimates, comparison with regional data and relationship to biogenic sedimentation. Global Biogeochem. Cycles **9**: 359–372.

Northern Economics, Inc., 2011. Executive Summary Update to 'The Seafood Industry in Alaska's Economy, 2009.' Prepared for the Marine Conservation Alliance, At-Sea Processors Association and Pacific Seafood Processors Association. Update sponsored by the Marine Conservation Alliance, Juneau, Alaska.

Palevsky, H. I., F. Ribalet, J. E. Swalwell, C. E. Cosca, E. D. Cokelet, R. A. Feely, E. V. Armbrust, and P. D. Quay. 2013. The influence of net community production and phytoplankton community structure on CO2 uptake in the Gulf of Alaska. Global Biogeochem. Cycles **27**: 664–676. doi:10.1002/gbc.20058

Poulton, S. W., and R. Raiswell. 2005. Chemical and physical characteristics of iron oxides in riverine and glacial meltwater sediments. Chem. Geol. **218**: 203–221. doi:10.1016/j.chemgeo.2005.01.007

Radic, A., F. Lacan, and J. W. Murray. 2011. Iron isotopes in the seawater of the equatorial Pacific Ocean: New constraints for the oceanic iron cycle. Earth Planet. Sci. Lett. **306**: 1–10. doi:10.1016/j.epsl.2011.03.015

Roy, E. G., M. L. Wells, D. W. King, and D. Whitney. 2008. Persistence of iron (II) in surface waters of the western subarctic Pacific. Limnol. Oceanogr. **53**: 89–98. doi:10.4319/lo.2008.53.1.0089

Royer, T. C. 1987. Coastal fresh water discharge in the northeast Pacific. **87**: 2017–2021.

Rudnick, R. L., and S. Gao. 2003. 3.01 - Composition of the Continental Crust. Treatise on Geochemistry 1: 1–64.

Schroth, A. W., J. Crusius, F. Chever, B. C. Bostick, and O. J. Rouxel. 2011. Glacial influence on the geochemistry of riverine iron fluxes to the Gulf of Alaska and effects of deglacation. Geophys. Res. Lett. **38**: 1–6. doi:10.1029/2011GL048367

Schroth, A. W., J. Crusius, I. Hoyer, and R. Campbell. 2014. Estuarine removal of glacial iron and implications for iron fluxes to the ocean. Geophys. Res. Lett. 1065–1070.

Sholkovitz, E. R. 1976. Flocculation of dissolved organic and inorganic matter during the mixing of river water and seawater. Geochim. Cosmochim. Acta **40**: 831–845. doi:10.1016/0016-7037(76)90035-1

Stabeno, P. J., N. A. Bond, A. J. Hermann, N. B. Kachel, C. W. Mordy, and J. E. Overland. 2004. Meteorology and oceanography of the Northern Gulf of Alaska. Cont. Shelf Res. **24**: 859–897. doi:10.1016/j.csr.2004.02.007

Stabeno, P. J., N. A. Bond, N. B. Kachel, C. Ladd, C. W. Mordy, and S. L. Strom. 2016a. Southeast Alaskan shelf from southern tip of Baranof Island to Kayak Island: Currents, mixing and chlorophyll-a. Deep. Res. Part II Top. Stud. Oceanogr. **132**: 6–23. doi:10.1016/j.dsr2.2015.06.018

Stabeno, P. J., S. Bell, W. Cheng, S. Danielson, N. B. Kachel, and C. W. Mordy. 2016b. Long-term observations of Alaska Coastal Current in the northern Gulf of Alaska. Deep. Res. II. **132**: 24–40. doi:10.1016/j.dsr2.2015.12.016

Strom, S. L., M. B. Olson, E. L. Macri, and C. W. Mordy. 2007. Cross-shelf gradients in phytoplankton community structure, nutrient utilization, and growth rate in the coastal Gulf of Alaska. Mar. Ecol. Ser. **328**: 75–92. doi:Doi 10.3354/Meps328075

Strom, S. L., K. A. Fredrickson, and K. J. Bright. 2016. Deep-Sea Research II Spring phytoplankton in the eastern coastal Gulf of Alaska : Photosynthesis and production during high and low bloom years. Deep. Res. Part II **132**: 107–121. doi:10.1016/j.dsr2.2015.05.003

Taylor S. R. and McLennan S. M. The Continental Crust: Its Composition and Evolution. (Blackwell, 1985).

Tsunogai, S., Watanabe, S., Sato, T., 1999. Is there a "continental shelf pump" for the absorption of atmospheric CO2? Tellus 51, 701–712. doi:10.1034/j.1600-0889.1999.t01-2-00010.x

Weingartner, T. J., S. L. Danielson, and T. C. Royer. 2005. Freshwater variability and predictability in the Alaska Coastal Current. Deep. Res. II. **52**: 169–191. doi:10.1016/j.dsr2.2004.09.030

Weingartner, T., L. Eisner, G. L. Eckert, and S. Danielson. 2009. Southeast Alaska: Oceanographic habitats and linkages. J. Biogeogr. **36**: 387–400. doi:10.1111/j.1365-2699.2008.01994.x

Wells, M. L., N. M. Price, and K. W. Bruland. 1995. Iron chemistry in seawater and its relationship to phytoplankton: A workshop report. Mar. Chem. 48: 157–182.

Wu, J. 2007. Determination of picomolar iron in seawater by double $Mg(OH)_2$ precipitation isotope dilution high-resolution ICPMS. Mar. Chem. 103: 370–381.

Wu, J., A. Aguilar-Islas, R. Rember, T. Weingartner, S. Danielson, and T. Whitledge. 2009. Size-fractionated iron distribution on the northern Gulf of Alaska. Geophys. Res. Lett. **36**: 1–4. doi:10.1029/2009GL038304

Yasunari, T. J., T. Shiraiwa, S. Kanamori, Y. Fujii, M. Igarashi, K. Yamazaki, C. S. Benson, and T. Hondoh. 2007. Intra-annual variations in atmospheric dust and tritium in the North Pacific region detected from an ice core from Mount Wrangell, Alaska. J. Geophys. Res. Atmos. **112**: 1–16. doi:10.1029/2006JD008121

Zdanowicz, C., G. Hall, J. Vaive, Y. Amelin, J. Percival, I. Girard, P. Biscaye, and A. Bory. 2006. Asian dustfall in the St. Elias Mountains, Yukon, Canada. Geochim. Cosmochim. Acta **70**: 3493–3507. doi:10.1016/j.gca.2006.05.005